This is a “preproof” accepted article for *Mineralogical Magazine*.
This version may be subject to change during the production process.
10.1180/mgm.2024.92

The morphology and spectroscopy of diamonds recovered from the Prairie Creek lamproite in Arkansas, USA.

R. Bassoo[1,2], S. Eaton-Magaña[1], M.F. Hardman[1], C.M. Breeding[1], K. Befus[3], J.E. Shigley[1]

[1]Gemological Institute of America, 5345 Armada Drive, Carlsbad, CA, 92008,

[2]Baylor University – One Bear Place, Waco, TX, USA, 76798., [3]University of Texas at Austin, Department of Earth and Planetary Sciences, 2515 Speedway, Austin, TX, USA, 78712.

Abstract

Diamonds are found occasionally in the United States of America. Diamonds from the Prairie Creek lamproite in Arkansas, USA occur within a north to south corridor of Neoproterozoic to mid-Cretaceous magmatism that extends across North America. These diamond bearing lamproites are unusual because they intrude adjacent to sutured and strongly thinned lithosphere rather than stable within-plate settings and the diamonds themselves provide physical evidence of processes related to diamond formation at the cratonic margin. Indeed, a review of previously published geophysical data, isotopic compositions, inclusion suites and inclusion geochemistry suggest most diamonds were formed in subducted and eclogitic rocks within a highly localized diamondiferous lithosphere beneath the cratonic margin. The morphology and spectroscopic character of 155 diamonds from the Prairie Creek lamproite suggest typical diamond formation

conditions in an otherwise thinned continental lithosphere. Most diamonds examined during this study have spectroscopic features indicating strong nitrogen aggregation, a history of thermal perturbation and plastic deformation. Nitrogen contents range up to 1882 ppm and the diamonds preserve ~ 70% aggregated nitrogen in the B aggregation state. Furthermore, inclusion elastic barometry and time averaged mantle residence temperatures suggest most Arkansas diamonds formed at 5.2±0.2 GPa and 1205±63 °C (1σ). However, a subpopulation ~ 4% of relatively large and inclusion free, colourless, flattened-to-irregular habit Arkansas diamonds are Type IIa with <5 at.ppm nitrogen. Those stones size, morphology, colour and N content might warrant their inclusion in the class of Cullinan-like, Large, Inclusion-Poor, Pure, Irregular and Resorbed or "CLIPPIR" diamonds. Other diamonds examined commonly exhibit physical evidence of plastic deformation, including brown body colour and deformation lamellae.

Keywords: Diamonds, Prairie Creek, North American Craton, kimberlite, lamproite.

Introduction

North America hosts numerous diamond deposits (Figure 1), with the most productive being in the northern regions of Canada. Many of these diamonds are sourced directly from kimberlites whereas others come from secondary glacial till deposits (e.g. Kjarsgaard and Levinson 2002). Though not as prolific as Canadian deposits, diamond occurrences found within the United States have yielded ~ 27,000 cts to-date. About 25% of those stones have been gem quality. Although most diamonds have been ≤ 2 ct, stones range up to 41 carats (Hausel 1994; Hausel 1998; Worthington 2007; Howard 2017; Wallace Jr 2017). Notable faceted gems include the 12.40 ct faint pinkish brownish, "M" colour grade 'Uncle Sam' diamond from Arkansas,

currently on display at the Smithsonian Institution in Washington DC. Another notable diamond is the 16.87 ct faint yellow, "L" colour grade 'Freedom' diamond from Colorado (Figure 2).

Diamonds from Arkansas are not a strong economic resource, but they drive significant tourism at the Crater of Diamonds State Park (Bassoo and Befus 2020). These diamonds are also important scientific resources, because they are ancient minerals from the mantle that are useful to infer mantle conditions and tectonic processes operating beneath the southern edge of the North American Craton. In the scientific literature, Arkansas diamonds are also known as Prairie Creek diamonds, referring to the Prairie Creek lamproite. No comprehensive studies exist that characterize the physical and spectroscopic characteristics of a large collection of Arkansas diamonds. Here, we review published isotopic and elemental compositions of these diamonds as well as their mineral inclusions. We then supplement this information with new data on the crystal morphology, infrared spectroscopy, elastic thermobarometry, optical cathodoluminescence, visible-near infrared absorption and photoluminescence spectroscopy of 155 diamonds from the Prairie Creek lamproite in Arkansas, which inform us of formation and deformation processes. We present new evidence indicating that diamonds from Arkansas formed in highly heterogeneous lithospheric mantle and subsequently underwent internal deformation. These processes may be characteristic of primary diamond occurrences along cratonic margins, as opposed to the more common kimberlite occurrences within cratons.

Geologic setting

Diamonds from the USA are found in placers and in Neoproterozoic to mid-Cretaceous-aged kimberlites and lamproites. Placer diamonds occur in the USA within Eocene to recent conglomerates and glacial moraines coincident with the proposed maximum extent of the

Laurentide glacial ice-sheet (Hobbs, 1899; Levinson et al., 1992; Hausel et al., 1994, Hausel and Bond 1994). Whereas the majority of global diamond-bearing igneous rocks typically penetrate through the thick, cold roots beneath ancient cratons, diamonds found in Arkansas lamproites occur in a distinct tectonic setting along the edge of the North American lithosphere. Recent geophysical studies indicate the lithosphere thins significantly to less than 150 km towards the south and southwest into the United States (Foster et al., 2013; Schaeffer and Lebedev 2014; Kjarsgaard et al., 2017). This is an atypical tectonic environment for diamond formation. Typically, old and thick cratons overlie Archean lithospheric roots that extend to 150 to 200 km in depth. Igneous rocks within these cratonic roots are depleted in Al, Ca, Fe, K, Th and U and are therefore relatively buoyant and cooler than the convecting mantle at similar depths (Jordan 1978; Pollack and Chapman 1977). These conditions raise the graphite to diamond phase transition to shallower depths, making the cratonic root favorable for diamond formation and storage (Stachel and Harris 2008). Outside of this narrow diamond stability field, we do not expect diamonds to form and/or reside for very long periods before turning to graphite. Consequently, diamondiferous kimberlites are typically found inside the oldest and thickest portions of cratons, where they transect the cratonic root and entrain diamonds (Smith 1983; Zurevinski et al., 2011; Stachel and Harris 2008). Kimberlites and lamproites that intrude along the margin of cratons should be devoid of diamonds because they do not transect this root zone (Kjarsgaard et al., 2022). Notable exceptions include the Buffalo Head Hills kimberlites in Canada, the Pimenta Bueno and Juína kimberlites in Brazil, and the Argyle and Ellendale lamproites in Australia (Jacques et al., 1989; Carlson et al., 1999; Bulanova et al., 2008; Luguet et al., 2009; Smit et al., 2010; Stachel et al., 2018; Jacques et al., 2018; Cabral-Neto et al., 2024). Diamondiferous lamproites in Arkansas are additional examples of primary diamondiferous

rocks which occur along craton margins. These lamproites occur above the extent of the subducting Farallon slab, within a tentative mid-Cretaceous to Neoproterozoic corridor that extends from Somerset Island in Arctic Canada through central Saskatchewan and Alberta to Prairie Creek in Arkansas (Figure 1) (Sharp 1974; Heaman et al., 2003; 2004; Currie and Beaumont 2011; Duke et al., 2014; Kjarsgaard et al. 2017).

Primary diamonds from Arkansas

In 1842 an unexpected outcrop of "peridotite rock" was reported by geologist W.B. Powell crosscutting Lower Cretaceous sedimentary units in Southwestern Arkansas near the confluence of Prairie Creek and the Little Missouri River (Miser and Ross, 1923). Diamonds were occaisionally reported in Arkansas subsequently during the late 1800s, but the discovery locations were kept secret. The 'Prairie Creek peridotite', now known to be a lamproite, was examined by geologist J.C. Branner in the late 1880s but no diamonds were found (Branner and Brackett, 1889). Diamonds were first formally discovered in 1906 at this locality when local farmer J.W. Huddleston found 2 stones, a ~3.0 ct white and a ~1.5 ct yellow, although accounts of this discovery vary (Henderson, 2002). Announcement of the discovery produced a speculative mining rush to the Prairie Creek area and led to the first scientific descriptions of Arkansas diamonds (e.g., Kunz and Washington, 1907). Decades of ensuing exploration and financially unsuccessful mining ventures at the Prairie Creek lamproite and in the surrounding area revealed additional lamproites, including the Twin Knobs #1, Twin Knobs #2, Black Lick, American and American North pipes. Each of these lamproites contain diamonds but they have not been economic to mine because of low diamond grades and sizes. The Prairie Creek lamproite had the highest diamond grade, but mining operations there, also never returned a

profit. In 1972, the State of Arkansas purchased the land the Prairie Creek lamproite occurs within and developed the Crater of Diamonds State Park. The state park is the only place in the world where the public can prospect a primary diamond deposit. Tourist and local artisanal miners recover ~600 stones per year, but only 3.5% are larger than 1 ct. The Prairie Creek lamproite which hosts these diamonds is located tectonically positioned between the Cenozoic Gulf Coastal Plain and the Paleozoic Ouachita Mountains (Dunn, 2003). They intrude the Upper Early Cretaceous Trinity Group of sediments and are unconformably overlain by the Lower Late Cretaceous Tokio Formation. Such stratigraphic constraints are confirmed by phlogopite $^{40}Ar/^{39}Ar$ ages of 99±2 Ma and 108±3 Ma, which indicate Cretaceous emplacement and crystallization of the lamproite (Zartman, 1977; Gogineni et al. 1978). Furthermore, radiogenic Sr (0.7069-0.771) suggest derivation from the sub-continental lithospheric mantle (SCLM) (Alibert and Albarède 1988; Heaman 1989; Lambert et al., 1995; Duke et al., 2024).

The reported lamproites have a variety of hypabyssal to subaerially-deposited facies, including magmatic, bedded volcanic breccias and tuffs and epiclastic deposits (Scott-Smith and Skinner, 1984; Walker 1991). All units are olivine lamproite and generally preserve an assemblage of olivine (Fo_{92}), clinopyroxene, poikilitic phlogopite, priderite, K-richterite, garnet, diamond, chromite and ilmenite. Much of the groundmass in all facies is thoroughly serpentinized. All facies contain abundant crustal xenoliths, as well as less common mantle eclogite, harzburgite, lherzolite and websterite xenoliths. Most diamonds are small (<2.0 mm); they have dodecahedral habits, but rare octahedral, tetrahexahedral and macle crystal habits are also found. The crystals can be colourless, light brown, or yellow. Diamonds frequently display fine hillocks and low-relief surfaces indicating intense or prolonged resorption (Waldman et al., 1987; McCandless et al., 1989). Isotopically, macro-diamonds from the Prairie Creek lamproite have mean $\delta^{13}C$ ~ -

6.5±2.8 ‰ which suggests formation from fluids derived from peridotitic rocks (McCandless et al., 1991; Cartigny 2005). Microdiamonds from Praire Creek lamproite with $\delta^{13}C$ values of -25.2 and -26.1 ‰ may indicate diamond crystallization from websteritic or eclogitic rocks (Deines and Harris, 2004; Ickert et al., 2013; Stachel et al. 2022).

Materials and Methods

Diamonds unearthed within the United States are either in inaccessible personal collections or are very expensive to acquire, even for stones with little value in the jewelry trade. Our collection of 155 diamonds from the Prairie Creek lamproite includes 7 diamonds that we found by personally mining on-site at the state park, 16 diamonds purchased from diamond dealer K. Glasser (Diamond Rough^{TM}) and 132 lent to us for study by local Arkansas miners/collectors, including Troy Savage, Glenn Worthington, Scott Kreykes, Sam Johnson, Don Roeder, Dennis Dunn and Tom Paradise.

The morphology and optical character of the diamonds was examined using a Zeiss AXIO petrographic microscope. These petrographic observations were used to characterize crystal shape, dissolution textures and abrasion. Additional visual inspection revealed diamond colour, colour distribution and presence/absence of mineral inclusions.

Infrared absorbance (IR) of the diamonds measured at GIA was accomplished using a ThermoFisher Scientific Nicolet iN10 FTIR spectrometer. Analyses were performed across 675-4000 cm^{-1} in cooled transmission mode using a 200 x 200 µm aperture size, 64 to 128 scans and a spectral resolution of 4 cm^{-1}. Some collectors preferred that their diamonds remain in their possession. For these 23 stones we used a transportable ThermoFisher Scientific IS5 FTIR. These analyses were performed across 675-4000 cm^{-1} at room temperature and a spectral

resolution of 4 cm^{-1}. For all samples nitrogen concentrations and aggregation state were calculated from individual spectra by applying the Beer-Lambert law and absorption values of the nitrogen bands at 1365, 1284 and 1175 cm^{-1}, using the least-squares fitting approach (Boyd et al., 1994; Boyd et al., 1995; Kiflawi et al., 1994; Howell et al. 2012a; 2012b). Individual total N concentration (at.ppm) vs. $\%N_B$ (degree of nitrogen aggregation from A to B centers) ratios were used to calculate mean residence temperatures using the kinetics of the nitrogen A-B center aggregation reaction (e.g., Taylor et al., 1990, 1996). Infrared spectra were also used to characterize diamond optical defects following Shigley and Breeding (2013).

Optical cathodoluminescence of diamonds was observed using a Nikon LV UEPI microscope equipped with a low vacuum Reliotron III cathodoluminescence system operated at 7.5-9 kV and 0.3-0.5 amps. For each diamond the luminescence colour response, or lack thereof, was documented during cathodoluminescence. The visible-near-infrared (vis-NIR) absorption spectra of diamonds were acquired by a GIA vis-NIR system at 77 K. Photoluminescence spectra of diamonds were acquired using a Renishaw inVia Raman microscope at 100% laser power, 5-10X magnification, a ~2 µm spot size, a full-resolution grating and with 457, 514, 633 and 830 nm laser excitations. The samples were kept at ~77 K during analyses.

Raman spectra of diamond-hosted inclusions were collected at Baylor University using a ThermoFisher Scientific DXR Raman microscope equipped with a 532 nm laser operating at 8 mW, a ~2 µm spot and a high-resolution grating (1800 lines mm^{-1}). Petrographic inclusion identification was confirmed with Raman spectra by matching peak positions and heights of the inclusions' spectra with those in the RRUFF spectral database (e.g., Lafuente et al., 2016). The Raman spectra of diamond-hosted inclusions were also used to calculate their entrapment pressures using elastic thermobarometry following Angel et al. (2017) and the thermobarometry

calculator provided by Befus and Cisneros (2020). Briefly, the shape and position of Raman spectra are a consequence of the mineral's crystal lattice environment. The positions of Raman bands, or peaks, in the spectra of a mineral are also proportional to the residual pressure preserved within the inclusion. Variations in residual pressure preserved in fully entrapped or liberated inclusions will cause a "peak shift" to higher or lower wavenumbers (e.g., Izraeli et al., 1999). Such peak shifts have been calibrated to calculate residual pressures in mantle minerals (McSkimin and Andreatch, 1972; Liu et al., 1991; Izraeli et al., 1999; Kohn, 2014). As a diamond is transported to the surface, the reduced pressure and temperature conditions cause inclusions to change volume and may impart an elastic strain against the rigid diamond. The rigid covalent bonding in diamond accounts for its extreme hardness and high incompressibility with a bulk modulus of 440 GPa at 300 K (Oganov et al., 2013). Diamond will therefore have a negligible volume change, making it a very rigid host and excellent recorder of entrapment pressures. Entrapment pressure is calculated from the measured residual pressure using an elastic model that accounts for the thermal expansivity and compressibility of diamond host and inclusion (e.g., Izraeli et al., 1999; Angel et al., 2017).

We analyzed forsterite and coesite inclusions in colourless diamond interiors, far from surface cracks. Peak shifts of entrapped inclusions were measured against the Raman spectra of the reference standard San Carlos olivine, ~Fo_{90} (Abramson et al., 1997). We also assume that the reference peak position of synthetic coesite is 521 cm^{-1}, 466 cm^{-1}, 427 cm^{-1}, 355 cm^{-1} (Hemley et al., 1984; Sobolev et al., 2000). We recognize a more precise residual pressure might be estimated by comparing to the measured peak position of a liberated coesite inclusion, but sample destruction was not possible for diamonds loaned for study. The resulting uncertainty in the calculated inclusion pressures has a 1σ standard error of ~0.6 GPa, which is controlled by the

1 cm^{-1} resolution of the Raman spectrometer. We acknowledge that diamond hosts may also have been plastically deformed, which can manifest as homogenous or banded pink-to-brown body colours and/or deformation "strain" lamellae. However, we did not acquire inclusion spectra from diamonds that exhibit these deformation traits, from locations near fractures, or close to the edge of the diamond surface. The selected inclusions were cubo-octahedral in shape. (e.g., Eaton-Magaña et al., 2018).

Results

Morphology and inclusions

Prairie Creek lamproite diamonds from Arkansas used in this study range in mass from ≤0.1 to 8.66 cts (mean 0.45±1.1 cts). Collectively, these diamonds were of colourless (59%), brown (30%), or yellow (11%) body colours (Figure 3). Many of these diamonds are fragments and their original morphology is unknown (30%). The remaining are dodecahedral to flattened dodecahedral (61%), combination (10%) and octahedral (3%) habits (Table 1). Approximately 20% of all diamonds preserve deformation lamellae which penetrate the crystal. A subset of 4% of diamonds from Arkansas are colourless, strongly resorbed, relatively larger and irregular to flattened in habit. Hillocks and terraces on crystal surfaces are common (Figure 4). Other dissolution features include flat-bottomed dissolution pits such as trigons and trapezoids, which account for 21% of diamonds examined. Diamonds from Arkansas also preserve flat-bottomed hexagon dissolution pits accounting for 5% of the population. Point bottom dissolution features were observed in one diamond. A quarter of the diamonds have frosted surfaces with corrosion sculptures or have visible microdisc swarms (9%). Diamonds from Arkansas have large cavities and minor edge abrasion (24%). Mineral inclusions were identified with Raman spectra.

Inclusions occur in 7% of Arkansas diamonds and are in order of decreasing abundance; diopside, rutile, magnetite, forsterite and coesite. Epigenetic graphite and grey to black with metallic luster sulfide inclusions also occur. However, no silicate inclusions were observed in the colourless, strongly resorbed, relatively larger and irregular to flattened in habit sub population of diamonds.

Cathodoluminescence

We applied optical cathodoluminescence to a group of 87 Arkansas diamonds. These diamonds cathodoluminesce green-blue, green and blue (53%, 24% and 15%, respectively). The remaining 8% of Arkansas diamonds are inert (Figure 5).

Photoluminescence and Visible-Near Infrared Absorption

Photoluminescence (PL) spectral peak positions of diamonds are associated with nitrogen content and aggregation state as well as various atomic-level structural defects, including interstitial carbon atoms, carbon vacancies, nitrogen impurities, nickel impurities, radiation damage and plastic deformation (Figure 6, Table 2). Complex nitrogen defects are pervasive in the photoluminescence spectra of all diamonds which are dominated by H4 (four substitutional nitrogen atoms surrounding two vacancies) and H3 (two substitutional nitrogen atoms separated by a vacancy) defects. Most diamonds have H3, NV^- (nitrogen-vacancy defect with negative charge) and NV^0 (nitrogen-vacancy with neutral charge state) defects. Nickel-related defects occur in almost half the diamond population. No more than 40% of diamonds preserve defects commonly associated with exposure to natural sources of radiation, with 38% having detectable GR1 740.9 and 744.4 nm (vacancy with neutral charge state) and 23% having 488.9 nm

(carbon/nitrogen-related interstitial) defects. More than 45% of diamonds have PL peaks related to defects caused by plastic deformation, including peaks at 490.7 nm and 576 nm. About 14% of Arkansas diamonds have Cape spectrum features and these stones never have detectable H3 defects (Table 3). More than 70% of Arkansas diamonds have featureless visible spectra (Figure 6). Only two Arkansas diamonds have a 550 nm absorption band.

Infrared spectroscopy

The nitrogen concentration in diamonds from Arkansas ranges between trace (<5 at.ppm ~ nominally Type IIa) and 1882 at.ppm, with a mean of 344 at.ppm (Table 1). As a whole, approximately 53% of the diamonds are Type IaAB with fewer Type IaA (20%), Type IaB stones (12%) and Type Ib stones (2%). Type IIa diamonds account for 12% of the diamond population. Of these Type IIa diamonds, 4% (n = 6) are larger (>0.7 cts), colourless, strongly resorbed and irregular. Infrared spectroscopy can be used to calculate the proportion of nitrogen A centers (N_A, pairs of substitutional nitrogen) relative to more aggregated or complex nitrogen B centers (N_B, four substitutional nitrogen surrounding a vacancy), using the absorption coefficients of N_A and N_B centers at 1282 $cm^{-1}$and 1175 cm^{-1}, respectively. Arkansas diamonds have a wide range of nitrogen aggregation states from weakly to strongly aggregated. The majority of the studied diamonds have >50% N_B (Figure 7A).

More than 85% of Arkansas diamonds have a hydrogen-nitrogen-vacancy defect center absorption at 3107 cm^{-1} (e.g., N3VH; Goss et al., 2014). The integrated absorbance at that wavenumber ranges from below detection (<0.05 cm^{-2}) to 13.9 cm^{-2} with a mean of 1.0±2.0 cm^{-2} (Table 1). When plotted against N_B concentrations our diamonds have integrated 3107 cm^{-1} peak areas much lower than the proposed "upper limit" of 3107 cm^{-1} areas (Figure 7B), which

correspond to the number of infrared-active N3VH centers (three substitutional nitrogen atoms surrounding a vacancy and a hydrogen atom). These defects are created as a by-product during N_A to N_B aggregation (Melton 2013).

The nitrogen aggregation state of diamonds can be used to calculate the temperature of the ambient mantle during diamond residence. Nitrogen A centers convert or aggregate to more complex B centers by diffusion over geologic time and at elevated temperature (e.g., Taylor et al., 1990, 1996). We determined mean diamond residence temperatures of 1205±63 ºC and a range from 1124 – 1321 °C assuming a mean formation age of 1.4 Ga between 1.6 Ga and 1.2 Ga or analogous to the inferred age of the SCLM of the Yavapai-Mazatzal terrane (Alibert and Albarède 1989, Lambert et al., 1995; Duke et al., 2014), and therefore a calculated residence time of 1.3 Ga. Varying the formation age between 1.6 Ga and 1.2 Ga varies the residence temperature by 1-3% (e.g. Channer 2001; Bassoo et al., 2021).

Many diamonds plot along isotherms ~1145 – 1190 °C (Figure 8) which is expected of cratonic diamonds (Stachel and Harris 2009). However, a sub-population of diamonds plot along warmer isotherms ~1215 – 1245 °C. Arkansas diamonds also have a small population of strongly aggregated IaB diamonds which indicate minimum residence temperatures of ~ 1320±0.4 °C, assuming 99% N_B aggregation (Figure 8).

Elastic thermobarometry

Previous studies of olivine and coesite inclusions in diamond indicate preserved residual pressures that range from ~2.8 to ~0.9 GPa respectively at room temperature. These residual pressures indicate inclusion entrapment pressures at depth from ~ 4.4 to 5.7 GPa at cratonic mantle temperatures (Izraeli et al., 1999; Sobolev et al., 2000; Bassoo et al., 2021b). Combined

Raman spectroscopic analyses and diamond residence temperatures of forsterite and coesite inclusions in Arkansas diamond inclusions record residual pressures from ~ -0.22 to 2.61 GPa. The single coesite inclusion records both negative and positive residual pressures indicating both tension and compression within it. We therefore assume anisotropy of coesite and do not extrapolate entrapment pressures. Forsterite inclusions indicate entrapment at 5.21±0.21 GPa and 1163±58 °C (Table 4). Such pressures and residence temperatures plot best along paleo-geotherms between 40 and 43 mW/m^2 (Figure 9).

Discussion

Tectonic setting

The "North American Craton" is a complex assemblage of Archean terranes sutured together by Proterozoic orogens (Hoffman 1988). Arkansas lamproites erupted through cratonic rocks of the 1.55 to 1.35 Ga Granite-Rhyolite Province, just to the south of the Mazatzal Province and north of the Grenville orogen (Figure 1) (Griffin et al., 2011). Diamond formation and storage within the subcontinental lithospheric mantle (SCLM) of the Yavapai-Mazatzal terrane seems unlikely because it generally does not exceed 150 km thickness. There are however, local seismic anomalies which may approach 200 km in depth today (Schaeffer and Lebedev 2014). Indeed, the Praire Creek lamproite at the time of eruption was likely underlain by a thick lithosphere which was at most 190 km. This is postulated to be the result of tectonic stacking of subcontinental lithospheric mantle rocks during terrane accretion and stabilization between 1.80 and 0.95 billion years ago beneath the southern edge of the Yavapai-Mazatzal terrane that has since thinned to its current depth (Griffin et al., 2004; Dunn, 2004; Whitmeyer and Karlstrom 2007).

Primary diamond occurrences along cratonic margins are rare but can be prospective to plastically deformed and fancy coloured pink, brown and violet diamonds, as is the case for the Ellendale and Argyle mine in northwestern Australia and the Bunder lamproite field in India (Hall and Smith, 1985; Jacques et al., 1989; Bulanova et al., 2008; Luguet et al., 2009; Gaillou et al., 2010; Smit et al., 2010; Eaton-Magaña et al., 2018; Smith et al. 2018; Stachel et al., 2018). Cratonic margins coincident with subducting slabs may create an environment favorable for plastic deformation of diamond and thus lead to the occurrence of diamonds with brown to pink colours. The transition between relatively thick and thinned lithosphere is conducive to the formation of edge-driven convection cells, generated by subducting and descending oceanic slabs (Elder 1976; King and Anderson 1998; Usui et al., 2003; Kjarsgaard et al., 2017). This dynamic tectonic environment in a highly viscous upper mantle could be the mechanism that deforms diamonds along the southern margin of the North American Craton. In some cases, upward migration of kimberlite and lamproite melts might also be facilitated by the leading edge of a subducting slab in an edge driven convection cell to then entrain diamonds from the lithosphere during their ascent to the surface (e.g. Barron et al., 1996; Griffin et al., 1998; Stachel et al., 2018). Indeed, Arkansas lamproites have emplacement ages which coincide with the Mesozoic subduction of the Farallon slab (Liu et al., 2008). However, it should be noted that diamondiferous rock associations with subduction may be entirely coincidental. We document physical and spectroscopic characteristics of Arkansas diamonds which may have formed in such mantle conditions and highlight a previously undescribed subpopulation of Arkansas diamonds which share traits in common with the CLIPPIR suite of diamonds.

Literataure review of Arkansas diamond-hosted inclusion compositions

Mineral inclusions within diamonds have compositions that reflect their mantle sources. We review previously published results in the context of our new analysis to better constrain diamond formation beneath the southern edge of the North American craton (Table 5). Inclusions suites from primary diamonds from Arkansas are predominantly eclogitic, including metallic sulphides with a minor proportion of peridotitic diamonds (Newton et al., 1977; Pantaleo et al., 1979; McCandless et al., 1991). Geochemical data for the inclusions is limited to single data points (Table 5). One low-Cr clinopyroxene inclusion in an Arkansas diamond had an Mg# of 87, which was lower than that expected for clinopyroxene derived from lherzolite and harzburgite (Newton et al. 1997). This inclusion also has relatively elevated concentrations of elements that are typically incompatible in mantle peridotite, including Na, K and Ti, when compared to global occurrences (Table A1). The presence of clinopyroxene, magnetite, psuedobrookite, magnetite inclusions and the sole clinopyroxene composition suggest an eclogitic paragenesis. Additionally, coesite and rutile cannot form in equilibrium with olivine in peridotitic mantle. Their presence as inclusions in Arkansas diamonds support the presence of subducted, metamorphosed and silica-oversaturated meta-basalts within the diamondiferous mantle beneath Arkansas (Schulze et al., 2013). The single olivine inclusion analyzed was low in Ca and preserved a Mg# of 93, placing it within the range expected for peridotitic rocks worldwide (McCandless et al., 1991; Stachel et al., 2022a). Additionally, only four olivine inclusions are recognized in three Arkansas diamonds thereby providing evidence for peridotite as a minor diamond host.

Isotopically, $\delta^{13}C$ values for diamonds from Arkansas have a mean $\delta^{13}C \sim -6\pm5$ ‰ and is within the range expected of both eclogitic and peridotitic diamond $\delta^{13}C$ values (Figure 10) (Stachel et al., 2022). Two diamonds with strongly depleted $\delta^{13}C < -21$‰ plot away from mantle

values. Previous modeling suggests values <-14 ‰ cannot be achieved by Rayleigh fractionation and are more likely related to recycled oceanic crust (Smart et al., 2011; Lai et al., 2022; Stachel et al., 2022b). Diamond composition, inclusion suites and geochemistry suggest subduction-influenced formation from eclogitic and possibly oceanic protoliths mixed with peridotitic rocks beneath the cratonic margin.

Formation and residence

Dodecahedral habits and common hillocks are physical features that indicate Arkansas diamonds experienced significant mantle and melt resorption. Most diamonds have flat bottomed dissolution, microdisc and corrosion sculpture textures which collectively indicate most diamonds were exposed to melts with a relatively high H_2O to CO_2 ratio (Tappert and Tappert, 2011; Fedortchouk, 2015). Hexagonal dissolution pits observed on one Arkansas diamond suggest at least some diamonds were also exposed to fluid compositions with $CO_2/(CO_2+H_2O)$ >0.9 during their ascent to the crust (Fedortchouk, 2019). About 30% of Arkansas diamonds preserve deformation lamellae and brown body colours, indicating they experienced plastic deformation in the mantle (Orlov 1977; Robinson et al., 1979; McCallum et al., 1991; Gaillou et al., 2010).

Paleo-thermobarometry of Diamond Formation

The diamonds examined in this study are from precious personal collections and we were not permitted to extract inclusions for study. Raman and infrared spectroscopy therefore offer alternative, non-destructive ways to calculate entrapment conditions where coexisting mineral pairs and assumptions of thermodynamic equilibrium are unavailable (e.g. Izraeli et al., 1999;

Angel et al., 2019, Stachel et al., 2022a). Forsterite and coesite inclusions in Arkansas diamonds record entrapment pressures ~ 5 GPa. Nitrogen aggregation suggests residence temperatures ranging from 1100 to 1220 °C. Pressure-temperature conditions estimated from inclusions in diamonds from Arkansas indicate typical formation conditions expected of cratonic diamonds globally (Stachel and Harris 2008). This is unexpected because independent geophysical studies corroborate formation within the craton margin and relatively shallow tectonic environments suggesting general thermal regimes unfavorable for diamond stability within the graphite field (Figure 8) (Foster et al., 2013; Schaeffer and Lebedev 2014; Kjarsgaard et al., 2017). However, pressure estimates ≥4.6 GPa from garnet lherzolite mantle xenoliths and garnet xenocrysts suggest the lithosphere beneath Arkansas may have been at most 190 km and possibly more laterally extensive, at the time of eruption of the Prairie Creek lamproite. (Dunn 2002, Griffin et al., 2004; Dunn 2004). Additionally, the timing of eruption is coincident with the subduction of the Farallon slab during the Mesozoic (Alibert and Albarède 1988; Heaman 1989; Lambert et al., 1995; Dunn 2002; Liu et al., 2008; Duke 2014). Subduction, therefore, may have played a role in subsequent thinning of the lithosphere beneath Arkansas to its current observable depth and lateral distribution. Hydrous partial melting during subduction could weaken the base of cratonic roots creating favorable conditions for delamination and lithospheric thinning (e.g., Liu et al., 2018; Shi et al., 2021). This is similarly observed at Argyle, Australia where diamonds are thought to form in a subduction-related tectonic regime (Figure 8) (Jaques et al., 2018; Timmerman et al., 2019).

Preservation of defects and diamond deformation

Photoluminescence, infrared and visible spectroscopy can be used to reveal diamond defects

related to formation conditions and subsequent tectonic activity, including deformation. Diamond is composed of carbon but intrinsic and extrinsic impurities can form during diamond growth, mantle residence, entrainment into ultramafic magmas and during lower-temperature residence in the crust. Impurity and vacancy related defects specifically inform us of diamond formation and residence.

Diamonds from Arkansas record spectroscopic evidence of Ni impurities. These impurities may have been incorporated during Ni-rich metasomatism of lithospheric mantle (Giuliani et al., 2013). Arkansas diamonds are nominally colourless, but <10% have a yellow colour caused by the presence of nitrogen (Shigley and Breeding, 2013). More than 25% of diamonds have complex nitrogen defects, and more than 50% of diamonds have >200 at.ppm N. They also tend to be more strongly aggregated in nitrogen than those at Argyle, which are also known to be derived from the craton margin (Figure 7A) (Bulanova et al., 2018). Indeed, based on nitrogen aggregation, a subpopulation of Arkansas diamonds record minimum residence temperatures ~1320 °C, indicating residence at very high temperatures for millions or billions of years, such as those that prevail in the base of the lithospheric mantle or uppermost asthenospheric mantle (Leahy and Taylor, 1997). In addition, most diamonds from Arkansas have a narrow range of N3VH peak area per N_B aggregation which is lower than that expected of diamonds from within craton settings, such as those analyzed from the Slave and Superior cratons, and is lower than Argyle (Figure 7B). Arkansas diamonds did not experience the maximum N3VH center creation as a consequence of A to B center aggregation (Melton 2013; Stachel et al., 2018; Bulanova et al., 2018). Diamonds from Arkansas instead indicate a lower concentration of available infrared-active hydrogen to accommodate N3 center creation (Melton 2013). These observations may suggest N_A to N_B aggregation is more efficient than the production of N3VH defects, which

might be caused by enhanced diffusion of nitrogen in diamond during plastic deformation and/or exposure to high thermal changes (Wood 1986; Evans 1992; Evans et al., 1995). Indeed, Arkansas diamonds preserve moderate incidences of plastic deformation related defects and a subpopulation of IaB diamonds which likely experienced exposure to high thermal perturbations (Evans et al., 1995).

About 30% of diamonds from Arkansas are brown with deformation lamellae and more than 45% have spectral features indicating that they experienced plastic deformation (Table 1; Table 2). Brown and pink colour in diamonds can manifest as a more uniform body colour or be concentrated within parallel narrow bands termed deformation lamellae. Brown colouration in diamond is related to vacancy clusters along the {111} plane and are interpreted to have formed by plastic deformation (Hounsome et al., 2006; Fisher et al., 2009; Gaillou et al., 2010; Eaton-Magaña et al., 2018). Applied stress altered the atomic structure of the diamond and created vacancies (Gaillou et al., 2010). Diamond defects responsible for brown body colours were likely acquired during their long residence up to 1 billion years and within the shallow lithospheric mantle at ~100 km (Collins 1982; Drury and Fitzgerald 1998; Collins et al., 2000; Gaillou 2010; Smith et al., 2010; Shirey and Shigley 2013). Furthermore, a population of 4% of Arkansas diamonds are relatively large (>0.7 cts.), inclusion poor, Type IIa with <5 at.ppm N, irregular to flattened in habit, strongly resorbed and colourless. Similarly non-faceted, large, colourless and irregular diamonds historically have been recovered from the Prairie Creek lamproite including the ~40 carat Uncle Sam and the ~15 carat Star of Arkansas (Leiper 1957). The relatively large size, strongly resorbed and irregular morphology, absence of colour and very low nitrogen content are traits shared by so-called CLIPPIR diamonds, which are inferred to be derived from sub-lithospheric depths and possibly as deeply as the transition zone or uppermost lower mantle

(Smith et al., 2016). Globally, CLIPPIR diamonds are rare, and comprise a small percentage of diamond populations. Of diamonds submitted to GIA for example, inclusion bearing CLIPPIR diamonds comprise 0.0001%. Examples of CLIPPIR diamonds have been recovered from the Premier and Letseng kimberlites, and potentially also the Argyle lamproite (Smith et al., 2016; Pay 2017; Smith et al., 2017; Stachel et al., 2018; Shirey et al., 2024).

Conclusions

Arkansas has moderate incidences of plastically deformed and potentially sub-lithospheric diamonds exposed to high temperature perturbations. Subduction processes may cause plastic deformation of a diamond entrained in a highly viscous and dynamic upper mantle. In this way subduction-driven tectonic settings may be more favorable for plastically deformed pink to brown diamonds along the margin of cratons. This has been similarly suggested for the Argyle mine, where diamonds might have originated from and deformed within the lithosphere-asthenosphere boundary (Stachel et al., 2018).

The Yavapai-Mazatzal terrane has isolated “pockets” of diamondiferous lithosphere and cratonic roots may have been more laterally extensive and extended to 190 km depth in the past (Griffin et al., 2004; Dunn 2004; Whitmeyer and Karlstrom 2007). A review of geochemical and geophysical data suggests that subsequent thinning of the lithosphere has left behind highly localized zones of mantle heterogeneity, depleted lithosphere and relatively thick mantle roots but within surrounding thinned lithosphere along the Southern margin of what constitutes the North American craton.

Arkansas has a sub-population of diamonds which are relatively large, largely inclusion free, strongly resorbed and Type IIa. These morphological and spectroscopic traits are shared with

sub-lithospheric CLIPPIR diamonds. Future studies to identify inclusion species and compositions within these diamonds could confirm CLIPPIR diamond occurrences in Arkansas.

Acknowledgments

We sincerely thank Dennis Dunn, Troy Savage, Don Roeder, Craig Zapf, Scott Kreykes, Tom Paradise and Glenn Worthington for their Arkansas diamond samples, insight into Prairie Creek geology and how to mine for diamonds. We are indebted also to Nathan Renfro, Emily Lane and Judy Colbert of the GIA for diamond photographs. We thank the reviewers for improving the quality of the article.

References

Abramson, E..H., Brown, J.M., Slutsky, L.J. and Zaug, J. (1997). The elastic constraints of San Carlos olivine to 17 GPa. Journal of Geophysical Research, 102, (B6), 12253-12263.

Alibert, C. and Albarède, F. (1988) Relationships between mineralogical, chemical and isotopic properties of some North American kimberlites. Journal of Geophysical Research, 93, (B7), 7643–7671.

Angel, R. J., Alvaro, M., & Nestola, F. (2017). 40 years of mineral elasticity: A critical review and a new parameterization of equations of state for mantle olivines and diamond inclusions. Physics and Chemistry of Minerals, 45, (2), 95–113.

Ashchepkov, I.V., Downes, H., Mitchell, R., Vladykin, N.V., Coopersmith, H., Palessky, S.V. (2013). Wyoming Craton Mantle Lithosphere: Reconstructions Based on Xenocrysts from Sloan and Kelsey Lake Kimberlites. (In) Proceedings of 10th International Kimberlite Conference. Springer, New Delhi.

Barron, L.M., Lishmund, S.R., Oakes, G.M., Barron, B.J. and Sutherland, F.L. (1996) Subduction model for the origin of some diamonds in the Phanerozoic of eastern New South Wales. Australian Journal of Earth Sciences, 43(3), 257-267.

Bassoo, R., Befus, K., Liang, P., Forman, S., & Sharman, G. (2021a) Deciphering the enigmatic origin of Guyana's diamonds. American Mineralogist, 106, (1), 54– 68.

Bassoo, R. and Befus, K. (2021b) Composition of the Sub-Cratonic Mantle of the Guiana Shield Inferred From Diamond-Hosted Inclusions. Geochemistry, Geophysics, Geosystems, 22(6), e2021GC009841.

Bassoo, R. and Befus, K. (2020) Finders, Keepers: Field Trip to Crater of Diamonds, USA. Gem News International, Gems and Gemology, 56(2), 311-314.

Bokii G.B., Bezrukov, G.N., Kluev Ju, A., Naletov, A.M., Nepsha, V.I (1986) Natural and Synthetic Diamonds. Nauka, Moscow

Branner, J.C. and Brackett, R.N., 1889, The peridotite of Pike County, Arkansas: American Journal of Science, Series 3,38, (223), 50-59.

Breeding, C.M., Eaton-Magaña, S. and Shigley, J.E. (2018) Natural-colour green diamonds: a beautiful conundrum. Gems and Gemology, 54(1), 3-27.

Bulanova, G.P., Smith, C.B., Walter, M.J., Blundy, J., Gobbo, L., EIMF, Kohn, S.C. (2008) Proto-kimberlitic ultra-deep diamonds from Collier 4 kimberlite pipe, Juina, Brazil. 9th International Kimberlite Conference Extended Abstract (9IKC-A-00227).

Bulanova, G.P., Speich, L., Smith, C.B., Gaillou, E., Kohn, S.C., Wibberley, E., Chapman, J.G., Howell, D., and Davy, A.T. (2018) The unique nature of Argyle fancy diamonds: Internal structure, paragenesis, and reasons for color. Society of Economic Geologists, Special Publication 20, 169-190.

Cabral-Neto, I., Ruberti, E., Pearson, D.G., Luo, Y., Azzone, R.G., Silveira, F.V., and Almeida, V.V. (2024) Diamond sources of the Juína region, Amazonian craton: textural and mineral chemical characteristics of Kimberley-type pyroclastic kimberlites. Mineralogy and Petrology, 118, 1–22.Carlson, S.M., Hillier, W.D., Hood, C.T., Pryde, R.P., Skelton, D.N. (1999) The Buffalo Hills kimberlites: a newly discovered diamondiferous kimberlite province in northcentral Alberta, Canada. Proceedings of the 7th Int. Kimberlite Conference, (1), 109–116.

Cartigny, P. (2005) Stable Isotopes and the Origin of Diamond. Elements, 1(2), 79–84.

Channer, D. M. DeR., Egorov, A., & Kaminsky, F. (2001). Geology and structure of the Guaniamo diamondiferous kimberlite sheets, South-West Venezuela. Revista Brasileira de Geociências, 31(4), 615–630.

Cisneros, M. and Befus, K.S. (2020). Applications and limitations of elastic thermobarometry: insights from elastic modeling of inclusion-host pairs and example case studies. Geochemistry, Geophysics, Geosystems, 21, (10), e2020GC009231.

Collins, A.T. (1982) Colour centres in diamond. Journal of Gemology, 18, (1), 37-75.

Collins, A.T., Kanda, H. and Kiflawi, H. (2000) Colour changes produced in natural brown diamonds by high-pressure, high-temperature treatment. Diamond and Related Materials, 9(2), 113-122.

Collins, A.T., Kanda, H., Isoja, J., Ammerlaan, C.A.J., van Wjk, J.A. (1998) Correlation between optical absorption and EPR in high-pressure diamond grown from a nickel solvent catalyst. Diamond and Related Materials, 7, (2/5), 333-338.

Currie, C. A. and C. Beaumont (2011), Are diamond-bearing cretaceous kimberlites related to low-angle subduction beneath western North America? Earth and Planetary Science Letters, 303, (1/2), 59–70.

Dalton, S., Stokes, C.R., and Batchelor, C.L. (2022) Evolution of the Laurentide and Innuitian ice sheets prior to the Last Glacial Maximum (115 ka to 25 ka). Earth-Science Reviews, 224, 103875.Day, H. W. (2012) A revised diamond-graphite transition curve. American Mineralogist, 97, (1), 52–62.

Deines, P. and Harris, J.W. (2004) New insights into the occurrence of 13C-depleted carbon in the mantle from two closely associated kimberlites: Letlhakane and Orapa, Botswana. Lithos, 77, (1/4), 125-142.

Drury, M.R. and FitzGerald J.D. (1998) Mantle Rheology: Insights from laboratory studies of deformation and phase transformation. In: The Earth's Mantle: Composition, Structure and Evolution, ed. by I. Jackson (Cambridge University Press, New York) pp. 503-559.

Dueker K, Yuan H.Y. and Zurek B (2001) Thick-structured Proterozoic lithosphere of the Rocky Mountain region. GSA Today 11, (12), 4–9

Duke, G. I., Carlson, R.W., Frost, C.D., Hearn Jr., B.C. and Eby, G.N. (2014) Continent- scale linearity of kimberlite-carbonatite magmatism, mid-continent North America. Earth and Planetary Science Letters, 403, 1–14.

Dunn, D. (2003) Xenolith mineralogy and geology of the Prairie Creek lamproite province, Arkansas. PhD thesis, University of Texas, Austin.

Dunn, D., Smith, D. and Bergman, S.C. (2002) Mantle xenoliths from the Prairie Creek Lamproite province, Arkansas, USA. 8th International Kimberlite Conference Long Abstract.

Dymshits, A.M., Sharygin, I.S., Malkovets, V.G., Yakovlev, I.V., Gibsher, A.A., Alifirova, T., Vorobei, S.S., Potapov, S.V. and Garanin, V.K. (2020). Thermal state, thickness and composition of the lithospheric mantle beneath the Upper Muna Kimberlite Field (Siberian Craton) constrained by clinopyroxene xenocrysts and comparison with Daldyn and Mirny

Fields. Minerals, 10(6), 549.

Eaton-Magaña, S., Ardon, T., Smit, K.V., Breeding, C.M. and Shigley, J.E. (2018) Natural-colour pink, purple, red and brown diamonds: band of many colours. Gems and Gemology, 54(4), 352-377.

Elder, J. (1976), The Bowels of the Earth, Oxford Univ. Press, Oxford, U. K.

Evans, T. (1992) Aggregation of nitrogen in diamond, in The properties of natural and synthetic diamond, Academic Press, London, 259–289.

Evans, T., Kiflawi, I., Luyten, W., Vantendeloo, G. and Woods, G.S. (1995) Conversion of platelets into dislocation loops and coidite formation in Type Iab diamonds: Proceedings of the Royal Society of London, Series A, , 449, (1936), 295–313.

Fedortchouk, Y. (2019) A new approach to understanding diamond surface features based on a review of experimental and natural diamond studies. Earth-Science Reviews, 193, 45-65.

Fedortchouk, Y. (2015) Diamond resorption features as a new method for examining conditions of kimberlite emplacement. Contributions to Mineralogy and Petrology, 170, (4), 36.

Fisher D., Sibley S.J., Kelly C.J. (2009) Brown colour in natural diamond and interaction between the brown related and other colour-inducing defects. Journal of Physics: Condensed Matter, 21, (36), 364213.

Foster, K., Dueker K., Schmandt B. and Yuan H. (2013), A sharp cratonic lithosphere-asthenosphere boundary beneath the American Midwest and its relation to mantle flow. Earth and Planetary Science Letters, 402, 82–89.

Gaillou E., Post J.E., Bassim N.D., Zaitsev A.M., Rose T., Fries M.D., Stroud R.M., Steele A., Butler J.E. (2010) Spectroscopic and microscopic characterizations of colour lamellae in natural pink diamonds. Diamond and Related Materials, 19, (10), 1217-1220.

Giuliani, A., Kamenetsky, V.S., Kendrick, M.A., Phillips, D. and Goemann, K. (2013) Nickel-rich metasomatism of the lithospheric mantle by pre-kimberlitic alkali-S–Cl-rich C–O–H fluids. Contributions to Mineralogy and Petrolpogy, 165, (1), 155–171.

Gogineni, S.V., Melton, C.E. and Giardini, A.A. (1978) Some petrological aspects of the Prairie Creek diamond-bearing kimberlite diatreme, Arkansas. Contributions to Mineralogy and Petrology, 66, (3), 251–261.

Griffin, W.L., O'Reilly, S.Y., Davies, R.M. (1998) Subduction-Related Diamond Deposits? Constraints, Possibilities and New Data from Eastern Australia. (In) Reviews in Economic Geology, Metamorphic and Metamorphogenic Ore Deposits, Frank M. Vokes, Brian Marshall, Paul G. Spry.

Griffin, W.L., O'Reilly, S.Y., Doyle, B.J., Pearson, N.J., Coopersmith, H., Kivi, K., Malkovets, V., Pokhilenko, N. (2004) Lithosphere mapping beneath the North American plate. Lithos, 77, 873-922.

Griffin, W. L., Begg, G. C., Dunn, D., O'Reilly, S. Y., Natapov, L. M., & Karlstrom, K. (2011). Archean lithospheric mantle beneath arkansas: continental growth by microcontinent accretion. *Bulletin of the Geological Society of America*, *123*(9-10), 1763-1775.

Grütter, H.S., Gurney, J.J., Menzies, A.H. and Winter, F. (2004) An updated classification scheme for mantle-derive garnet, for use by diamond explorers. Lithos, 77, 841-857.

Grütter, H.S., Apter, D.B. and Kong, J. (1999) Crust-mantle coupling: evidence from mantle derived xenocrystic garnets. In: Gurney, J.J., Gurney, J.L., Pascoe, M.D., Richardson, S.H. (Eds.), Proceedings of the Seventh International Kimberlite Conference, Vol.1, Red Roof Design, Cape Town, pp. 307–313.

Hall, A.E., and Smith, C.B.(1985)Lamproite diamonds—are they different?, in Glover, J.E, and Harris, P.G., eds., Kimberlite occurrence and origin: A basis for conceptual models in exploration: Perth, Geology Department and University Extension, University of Western Australia, 8, 167-212.

Hasterok, D. and Chapman, D. (2011) Heat production and geotherms for the continental lithosphere. Earth and Planetary Science Letters, 307, (1/2), 59-70.

Hausel, W.D. (1994) Pacific coast diamonds – An unconventional source terrane. Wyoming State Geological Survey mineral report MR94-8.

Hausel, W.D. (1998) Diamonds and mantle source rocks in the Wyoming Craton with a discussion of other U.S. occurrences. Wyoming State Geological Survey Report of Investigations No. 53, 93 pp

Hausel, W.D. and Bond, J .E. (1994) Appalachian diamonds- old discoveries- new frontier: International California Mining Journal, 64 (3), 36-37.

Heaman, L. M. (1989). The nature of the subcontinental mantle from Sr-Nd-Pb isotopic studies on kimberlitic perovskite. Earth and Planetary Science Letters, 92, (3/4), 323– 334.

Heaman, L. M., B. A. Kjarsgaard and R. A. Creaser (2004) The temporal evolution of North American kimberlites. Lithos, 76, 377–398.

Heaman, L. M., Kjarsgaard, B.A and Creaser, R.A. (2003) The Timing of Kimberlite Magmatism in North America: Implications for Global Kimberlite Genesis and Diamond Exploration. Lithos, 71, (2/4), 153–184.

Hemley, R.J. (1984) Pressure dependence of Raman spectra of SiO_2 polymorphs: alpha-quartz, coesite and stishovite, in: MH Manghnani, Y Syono (Eds.). High-pressure Research in Mineral Physics, Tokyo/Washington DC: Terra Scientific Publishing Co and AGU, 347-360.

Henderson, John C. (2002) “The Crater of Diamonds: A History of the Pike County, Arkansas, Diamond Field, 1906–1972.” PhD diss., University of North Texas.

Hobbs W.H. (1899) The diamond field of the Great Lakes. Journal of Geology, 7, (4), 375-388.

Hoffman, P. (1988) United Plates of North America, The Birth of a Craton: Early Proterozoic Assembly and Growth of Laurentia. Annual Review in Earth and Planetary Sciences, 16, 543-603

Hounsome L.S., Jones R., Martineau P.M., Fisher D., Shaw M.J., Briddon P.R., Oberg S. (2006) Origin of brown colouration in diamond. Physical Review B, 73(12), 125203.

Howard, J.M. (2017) Crater of Diamonds-The natural state’s gem of a park. (in) Bullock, E., Butler, J.E., Dunnell, K., Feigelson, B.N., Funk, M.T., Gaillou, E., Howard, J.M., Janse, B., Jaszczak, J.A., Koivula, J.I., Rossman, G.R., Skalwold, E.A., Shigley, J., Harris, J., Staebler, G.A., Scovil, J. and, Weldon, R. (2017) Diamond the ultimate gemstone. Lithographie Ltd. Arvada, Colourado.

Howell, D., O'Neill, C. J., Grant, K. J., Griffin, W. L., Pearson, N. J., & O'Reilly, S. Y. (2012a). μ-FTIR mapping: Distribution of impurities in different types of diamond growth. Diamond and Related Materials, 29, 29–36.

Howell, D., O'Neill, C. J., Grant, K. J., Griffin, W. L., Pearson, N. J., O'Reilly, S. Y., et al. (2012b). Platelet development in cuboid diamonds: Insights from micro-FTIR mapping. Contributions to Mineralogy and Petrology, 164(6), 1011–1025.

Iakoubovskii, K. and Adriaenssens, G.J. (1999) Photoluminescence in CVD diamond films. Physica Status Solidi (a), 172, (1), 123–129.

Ickert, R.B., Stachel, T., Stern, R.A. and Harris, J.W. (2013) Diamond from recycled crustal carbon documented by coupled $\delta^{18}O$–$\delta^{13}C$ measurements of diamonds and their inclusions,

Earth and Planetary Science Letters, 364, 85-97.

Izraeli, E. S., Harris, J. W., & Navon, O. (1999). Raman barometry of diamond formation. Earth and Planetary Science Letters, 173, (3), 351–360.

Jaques, A.L., Luguet, A., Smith, C.B., Pearson, D.G., Yaxley, G.M., and Kobussen, A.F. (2018) Nature of the mantle beneath the Argyle AK1 lamproite pipe: Constraints from mantle xenoliths, diamonds, and lamproite geochemistry. Society of Economic Geologists, Special Publication 20, 119-143.

Jaques, A. L., Hall, A. E., Sheraton, J., Smith, C. B., Sun, S.-S., Drew, R. M., et al. (1989). Composition of crystalline inclusions and C-isotopic composition of Argyle and Ellendale diamonds: Perth (Vol. 14, pp. 966-989). Geological Society of Australia Special Publication.

Smit, K.V., Shirey, S.B., Richardson, S.H., le Roex, A.P., and Gurney, J.J., 2010, Re-Os isotopic composition of peridotitic sulphide inclusions in diamonds from Ellendale, Australia: Age constraints on Kimberley cratonic lithosphere: Geochimica et Cosmochimica Acta, 74, 3292-3306.

Jordan, T.H., (1978). Composition and development of continental tectosphere. Nature 274, (5671), 544–548.

King, S. D. and D. L. Anderson (1998) Edge-driven convection, Earth and Planetary Science Letters, 160, (3/4), 289–296

Kjarsgaard B.A. and Levinson, A.A. (2002). Diamonds in Canada. Gems and Gemology, 38, (3), 208-238.

Kjarsgaard, B.A., Heaman, L.M., Sarkar, C. and Pearson, D.G. (2017) The North America mid-Cretaceous kimberlite corridor: Wet, edge-driven decompression melting of an OIB type deep mantle source. Geochemistry, Geophysics, Geosystems, 18, (7), 2727-2747.

Kjarsgaard, B. A., de Wit, M., Heaman, L. M., Pearson, D. G., Stiefenhofer, J., Janusczcak, N., Shirey, S. B. (2022). A review of the geology of global diamond mines and deposits. Reviews in Mineralogy and Geochemistry, 88(1), 1-117.

Kohn, M. J. (2014). "Thermoba-Raman-try": Calibration of spectroscopic barometers and thermometers for mineral inclusions. Earth and Planetary Science Letters, 388, 187–196.

Komarovskikh A, Dmitriev A, Nadolinny V, Palyanov Y (2017) A DFT calculation of EPR parameters of a germanium-vacancy defect in diamond. Diamonds and Related Materials 76, 86–89.

Kopylova, M.G., Russell, J.K. and Cookenboo, H. (1999) Petrology of peridotite and pyroxenite xenoliths from the Jericho Kimberlite: Implications for the thermal state of the mantle beneath the Slave Craton, Northern Canada, Journal of Petrology, 40, (1), 79-104.

Krajick, K. (2011) Barren Lands; an epic search for diamonds in the North American Arctic. iUniverse, 460 pp.

Kunz, G.F. (1885) Precious stones, Mineral resources of the United States: U.S. Geological Survey, 723-782.

Kunz, G.F. and H.S. Washington. (1908) Diamonds in Arkansas. Bulletin of the American Institute of Mining Engineers, 20, 1-8.

Kurosawa, M., Yurimoto, H., & Sueno, S. (1997). Patterns in the hydrogen and trace element compositions of mantle olivines. Physics and Chemistry of Minerals, *24*, 385–395.

Lafuente, B., Downs, R. T., Yang, H. and Stone, N. (2016) The power of databases: the RRUFF project. In Highlights in mineralogical crystallography (pp. 1-29). Walter de Gruyter GmbH.

Lambert, D.D., Shirey, S.B. and Bergman, S.C., (1995) Proterozoic lithospheric mantle source for the Prairie Creek lamproites: Re-Os and Sm-Nd isotopic evidence. Geology, 23 (3), 273-

276

Leahy, K. and Taylor, W.R. (1997) The influence of the Glennie domain deep structure on the diamonds in Saskatchewan kimberlites. Russian Geology and Geophysics, 38, 481-491.

Leiper, H. (1957) A description of some of the diamonds found in Arkansas. Journal of Gemmology, 6 (2), 63-71.

Levinson, A.A., Gurney, J.J., Kirkley, M. B. (1992) Diamond sources and production: Past, present and future. Gems & Gemology, 28 (4), 234–254.

Lindblom, J., Holsa, J., Papunen, H. and Hakkanen, H. (2005) Luminescence study of defects in synthetic as-grown and HPHT diamonds compared to natural diamonds. American Mineralogist, 90, 428–440.

Liu, L. G., Mernagh, T. P., Jaques, A. L. (1990). A mineralogical Raman spectroscopy study on eclogitic garnet inclusions in diamonds from Argyle. Contributions to Mineralogy and Petrology, 105, 156-161.

Liu, L., S. Spasojevic and M. Gurnis (2008) Reconstructing Farallon plate subduction Beneath North America Back to the Late Cretaceous, Science, 322, (5903), 934–938.

Liu, L., Morgan, J. P., Xu, Y., & Menzies, M. (2018a). Craton destruction part I: Cratonic keel delamination along a weak mid-lithospheric discontinuity layer. Journal of Geophysical Research: Solid Earth, 123, 10040–10068.

Luguet, A., Jaques, A.L., Pearson, D.G., Smith, C.B., Bulanova, G.P., Roffey, S.L., Rayner, M.J., Lorand, J.-P. (2009) An integrated petrological, geochemical and Re–Os isotope study of peridotite xenoliths from the Argyle lamproite, Western Australia and implications for cratonic diamond occurrences. Lithos, 112, (S2), 1096-1108.

McCallum, M.E., Huntley, P.M., Falk, R.W. and Otter, M.L. (1991) Morphological, resorption

and etch features trends of diamonds from kimberlites within the Colourado-Wyoming State Line district, USA. 5th International Kimberlite Conference, 5, 264-266.

McCandless, T.E. (1991) Macro- and microdiamonds from Arkansas lamproites: Morphology, inclusions and isotope geochemistry. 5th International Kimberlite Conference, 5, 264-266.

McSkimin, H. J., & Andreatch, P. (1972). Elastic moduli of diamond as a function of pressure and temperature. Journal of Applied Physics, 43, (7), 2944–2948.

Melton, G.L. (2013) Elemental impurities, defects and carbon isotopes in mantle diamonds: Ph.D. thesis, Edmonton, Canada, University of Alberta, 155 pp.

Miser, H.D. and Ross, C.S., 1923, Diamond-bearing peridotites in Pike County, Arkansas: U.S. Geological Survey Bull. 735-I , 279-322.

Malogolovets, V.G., Vishnevskii A.C., Samoilovich, M.I. (1979) Doklady Akademii Nauk Ukrainy SSR, Ser. A, No. 5, p-366.

Naeser, C. W. and McCallum, M. E. (1977) Fission-track dating of kimberlite zircons. Extended Abstracts, Second International Kimberlite Conference, Santa Fe, New Mexico.

Newton, M.G., Melton, C.E., Giardini, A.A. (1977) Mineral inclusions in an Arkansas diamond. American Mineralogist 62, (5-6), 583-586

Oganov, A., Hemley, R. J., Hazen, R. M., & Jones, A. P. (2013). Structure, Bonding and Mineralogy of Carbon at Extreme Conditions. Reviews in Mineralogy and Geochemistry, 75, 47–77.

Orlov, Y.L (1977) The Mineralogy of the Diamond. Wiley-Interscience, 236 pp.

Pantaleo, N.S., Newton, M.G., Gogineni, S.V., Melton, C.E. and Giardini, A.A. (1979) Mineral inclusions in four Arkansas diamonds: their nature and significance. American Mineralogist, 64, (9/10), 1059-1062.

Pay, D. (2017). Editorial: The World's Biggest Diamonds: Windows into the Earth's Deep Mantle. Gems and Gemology, 53(4), 387.

Pielou, E.C. (1991) After the Ice Age. University of Chicago Press, Chicago, 376 pp.

Pollack, H.N., Chapman, D.S., (1977). On the regional variation of heat flow, geotherms, and lithospheric thickness. Tectonophysics 38, (3/4), 279–296.

Robinson, D.N. (1979) Surface textures and other features of diamonds. Ph.D. thesis. University of Cape Town, Rondebosch. South Africa.

Schaeffer, A. J. and Lebedev, S. (2014) Imaging the North American continent using waveform inversion of global and US Array data. Earth and Planetary Science Letters, 402, 26–41.

Schulze, D.J., Harte, B., Page, F.Z., Valley, J.W., Channer, D.M.D., Jaques, A.L. and Edinburgh Ion Microprobe Facility (2013) Anti-correlation between low $\delta^{13}C$ of eclogitic diamonds and high $\delta^{18}O$ of their coesite and garnet inclusions requires a subduction origin: Geology, 41, (4), 455–458.

Scott-Smith, B.H. and Skinner, E.M.W. (1984) A new look at Prairie Creek, Arkansas, in Kimberlites and related rocks: Proceedings of the Third International Kimberlite Conference, Washington, D.C., American Geophysical Union, 1, 255-284.

Sharp, W. E. (1974), A plate tectonic origin for diamond-bearing kimberlite. Earth and Planetary Science Letters, 21, (4), 351–354

Shi, Y.-N., Li, Z.-H., Chen, L., & Morgan, J. P. (2021). Connection between a subcontinental plume and the mid-lithospheric discontinuity leads to fast and intense craton lithospheric thinning. Tectonics, 40, e2021TC006711.

Shigley, J.E. and Breeding, M. (2013) Optical defects in diamond: a quick reference chart. Gems and Gemology, 49 (2), 107-111.

Shirey, S.B., Pearson, D.G., Stachel, T., and Walter, M.J. (2024) Sublithospheric Diamonds: Plate Tectonics from Earth's Deepest Mantle Samples Annual Review of Earth and Planetary Sciences, 52, 249-293

Shirey, S.B., and Shigley, J.E. (2013). Recent advances in understanding the geology of diamonds. Gems and Gemology, 49(4), 188-222.

Smith, E., Helmstaedt, H., and Flemming, R., 2010, Survival of brown color in diamond during storage in the subcontinental lithospheric mantle: Canadian Mineralogist, v. 48, p. 571-582.

Smith E.M., Shirey S.B., Nestola F., Bullock E.S., Wang J., Richardson S.H. and Wang W. (2016) Large gem diamonds from metallic liquid in Earth's deep mantle. Science, 354, (6318), 1403-1405.

Smith, E., Shirey, S.B., and Wang, W. (2017). The very deep origin of the world's largest diamonds. Gems and Gemology, 53(4), 388-403.

Smith, C. B. (1983) Pb, Sr and Nd isotopic evidence for sources of southern African. Nature, 304, (5921), 51–54.

Smith, C.B., Bulanova, G.P., Kobussen, A.F., Burnham, A., Chapman, J.G., Davy, A.T., and Sinha, K.K. (2018) Diamonds from the Atri South pipe, Bunder lamproite field, India, and implications for the nature of the underlying mantle: Society of Economic Geologists, Special Publication 20, 237-252.

Smit, K.V., Shirey, S.B., Richardson, S.H., le Roex, A.P., and Gurney, J.J., 2010, Re-Os isotopic composition of peridotitic sulphide inclusions in diamonds from Ellendale, Australia: Age constraints on Kimberley cratonic lithosphere: Geochimica et Cosmochimica Acta, 74, 3292-3306.Sobolev, N.V., Fursenko, B.A., Goryainov, S.V., Shu, J., Hemley, R.J., Mao, H., Boyd,

F.R. (2000). Fossilized high pressure from the Earth's deep interior: The coesite-in-diamond barometer. Proceedings of the National Academy of Sciences, 97(22), 11875-11879.

Sobolev E. V., Lisoivan V. I. Impurity centers in diamond. Report of the 8th Conference on Inorganic Chemistry Inst. Novosibirsk, 1971.

Spasojevic, S., Liu, L. and Gurnis, M. (2009) Adjoint models of mantle convection with seismic, plate motion and stratigraphic constraints: North America since the Late Cretaceous. Geochemistry. Geophysics, Geosystems, 10, (5), Q05W02.

Stachel, T and Harris, J.W. (2009) Formation of diamond in the Earth's mantle. Journal of Physics: Condensed Matter, 21, (36), 364206.

Stachel, T. and Harris, J.W. (2008). The origin of cratonic diamonds – constraints from mineral inclusions. Ore Geology Reviews, 34, (1/2), 5-32.

Stachel, T., Harris, J. W., Hunt, L., Muehlenbachs, K., Kobussen, A.F. (2018) Argyle Diamonds: How Subduction Along the Kimberley Craton Edge Generated the World's Biggest Diamond Deposit. (In) Special Publication of the Society of Economic Geologists, Chapter 6. Geoscience and Exploration of the Argyle, Bunder, Diavik and Murowa and T. Davy, Chris B. Smith, H. Helmstaedt, A. Lynton Jaques, John J. Gurney.

Stachel, T., Aulback, S., Harris, J.W. (2022a). Mineral inclusions in lithospheric diamonds. Reviews in Mineralogy and Geochemistry, 88, 307-392.

Stachel, T., Cartigny, P., Chacko, T., & Pearson, D. G. (2022b). Carbon and nitrogen in mantle-derived diamonds. Reviews in Mineralogy and Geochemistry, 88, 809-875.

• Sudholz, Z. J., Jaques, A. L., Yaxley,G. M., Taylor, W. R., Czarnota, K., Haynes, M. W., et al. (2023). Mapping the structure and metasomatic enrichment of the lithospheric mantle beneath the Kimberley Craton, Western Australia. Geochemistry, Geophysics, Geosystems, 24,

e2023GC011040. https://doi.org/10.1029/2023GC011040Tappert, R. and Tappert, M.C. (2011) Diamonds in nature – A guide to rough diamonds. Springer , 142 pp.

Taylor, W. R., Canil, D., & Milledge, H. J. (1996). Kinetics of Ib to IaA nitrogen aggregation in diamond. Geochimica et Cosmochimica Acta, 60, (23), 4725–4733.

Taylor, W. R., Jaques, A. L., & Ridd, M. (1990). Nitrogen-defect aggregation characteristics of some Australasian diamonds: Time-temperature constrains on the source regions of pipe and alluvial diamonds. American Mineralogist, 75, (11/12), 1290–1310.

Timmerman, S., Honda, M., Zhang, X., Jaques, A. L., Bulanova, G., Smith, C. B., & Burnham, A. D. (2019). Contrasting noble gas compositions of peridotitic and eclogitic monocrystalline diamonds from the Argyle lamproite, Western Australia. Lithos, 344, 193-206.

Usui, T., Nakamura, E., Kobayashi, K., Maruyama, S., Helmstaedt, H. (2003) Fate of the subducted Farallon plate inferred from eclogite xenoliths in the Colourado Plateau. Geology, 31 (7), 589–592.

Waldman, M.A., McCandless, T.E. and Dummett, H.T. (1987) Geology and petrography of the Twin Knobs #2 lamproite. Pike County, Arkansas. Geological Society of America Special Paper, 215, 205-216.

Walker, E.C. (1991) Petrogenesis of the Prairie Creek, Arkansas, diamondiferous olivine lamproite. A Thesis submitted in conformity with the requirements for the degree of Doctorate of Philosophy, Department of Geology, University of Western Ontario.

Wallace Jr, T.C. (2017) Colourado Diamonds (in) Bullock, E., Butler, J.E., Dunnell, K.,Feigelson, B.N., Funk, M.T., Gaillou, E., Howard, J.M., Janse, B., Jaszczak, J.A., Koivula, J.I., Rossman, G.R., Skalwold, E.A., Shigley, J., Harris, J., Staebler, G.A., Scovil, J. and, Weldon, R. (2017) Diamond, the ultimate gemstone. Lithographie Ltd. Arvada, Colourado.

Wang, S.Y., Sharma, S.K. and Cooney, T.F. (1993). Micro-Raman and infrared spectral study of forsterite under high pressure. American Mineralogist, 78, (5/6), 469-476.

Westerlund K. J., Shirey S. B., Richardson S. H., Carlson R.W., Gurney J. J. and Harris J. W. (2006) A subduction wedge origin for Paleoarchean peridotitic diamonds and harzburgites from the Panda kimberlite, Slave craton: evidence from Re–Os isotope systematics. Contributions to Mineralogy and Petrology, 152, (3), 275–294.

Whitmeyer, S.J., and Karlstrom, K.E. (2007) Tectonic model for the Proterozoic growth of North America. Geosphere, 3 (4), 220–259.

Worthington, G. (2007) Genuine diamonds found in Arkansas. M.A.P./Mid-America Prospecting.

van Wyk, J.A. and Woods, G.S. (1995) Electron Spin Resonance of Exited States of the H3 and H4 Centers in Irradiated Type Ia Diamonds. Journal of Physics: Condensed Matter, 7, (29), 5901–5911.

Zaitsev, A.M. (2010) Optical properties of diamond: A data handbook. Springer-Verlag Berlin 502 pp.

Zartman, R.E. (1977) Geochronology of some alkalic rock provinces in eastern and central United States. Annual Reviews of Earth and Planetary Sciences, 5, 257–286.

Zurevinski, S. E., Heaman, L.M. and Creaser, R.A (2011) The origin of Triassic/Jurassic kimberlite magmatism, Canada: Two mantle sources revealed from the Sr-Nd isotopic composition of groundmass perovskite. Geochemistry, Geophysics, Geosystems, 12, (9), Q09005.

List of Figures

Figure 1. Kimberlite, lamproite and reported diamond occurrences in North America overlain with the maximum extent of the Laurentide ice-sheet, the Yavapai-Mazatzal terrane, Archean terranes and the eastern edge of the subducting Farallon slab at 100 and 90 Myr ago (Hoffman, 1988; Hausel 1998; Krajick 2011; Kjarsgaard et al., 2017; Czas 2018). Most diamond occurrences in the USA appear to be spatially coincident with the extent of the Laurentide ice sheet during the last glacial maximum (Pielou 1991; Dalton et al., 2022).

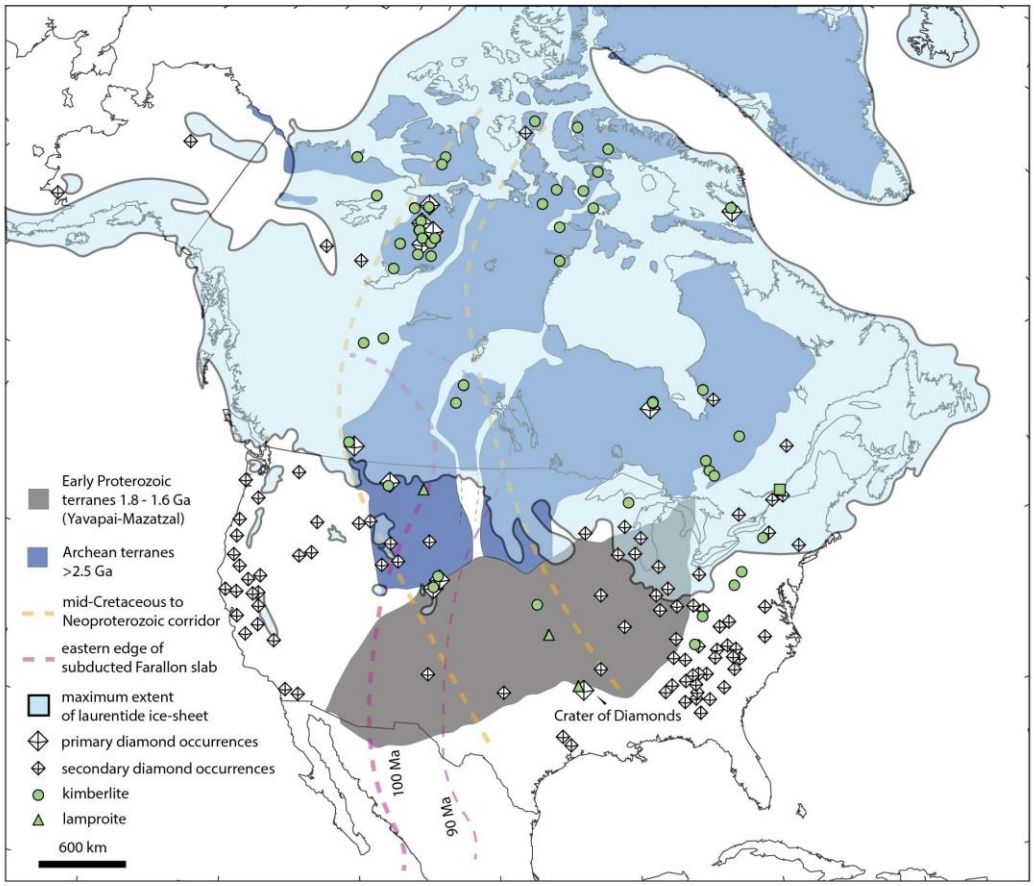

Figure 2. Famous diamonds found in the USA include the A) 16.87 ct. Colorado “Freedom”, B) 4.25 ct. Arkansas “Kahn Canary” set within a design by Henry Dunay and famously worn by Hillary Clinton, C) 12.40 ct. Arkansas “Uncle Sam” and D) a suite of six diamonds mined from the Prairie Creek lamproite by one of the most prolific local Arkansas diamond miners, James Archer and set within a brooch commissioned by Sue John Anthony. Photo credits to Smithsonian National Museum of Natural History for photographs of the Colorado Freedom and Uncle Sam, Glenn Worthington for the Kahn Canary and Nathan Renfro for the Sue John Anthony jewelry piece.

Figure 2

Figure 3. Selected diamonds from A) the Prairie Creek lamproite, Arkansas, including B) large colourless Type IIa varieties.

Figure 3

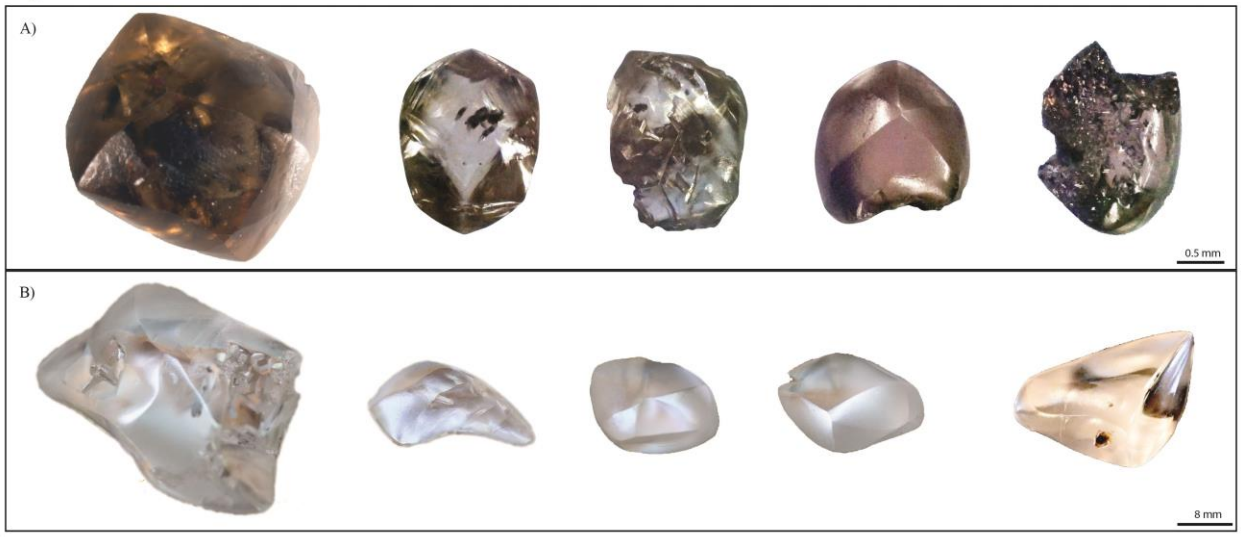

Figure 4. Surface textures and inclusions typical of diamonds from Arkansas.

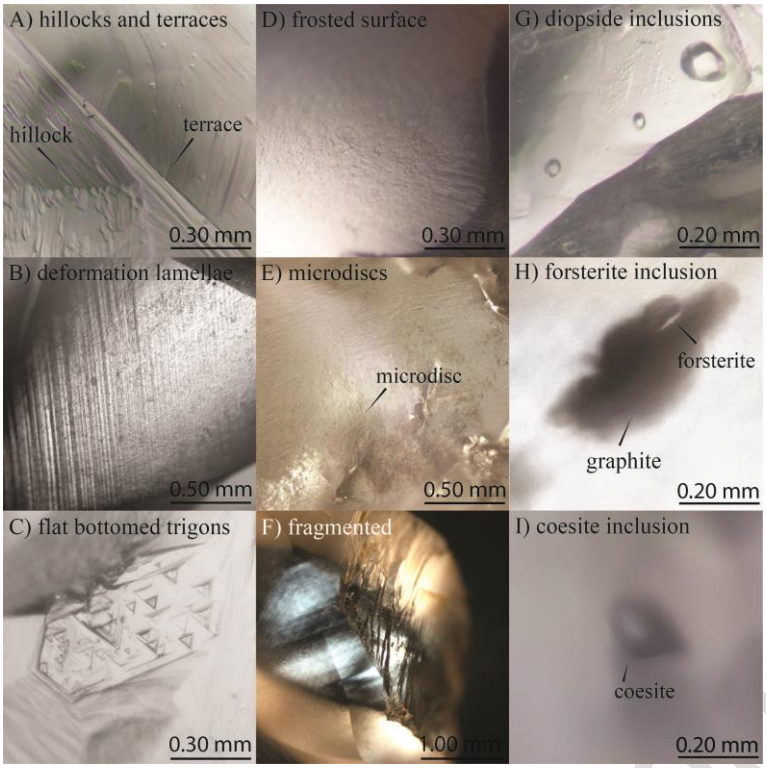

Figure 5. Cathodoluminescence colours and proportions observed in a subset of 87 Arkansas diamonds.

Figure 5

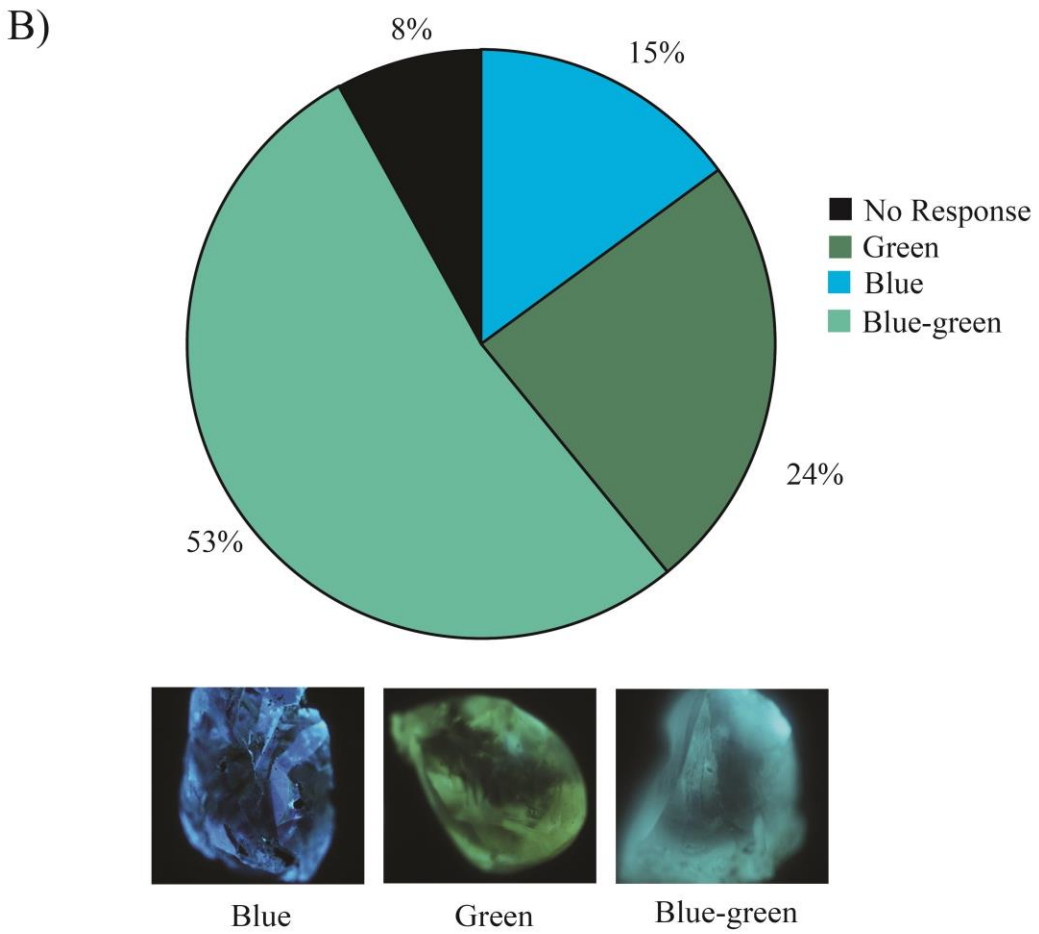

Figure 6. Representative photoluminescence (PL) and visible-near infrared (vis-NIR) spectra.

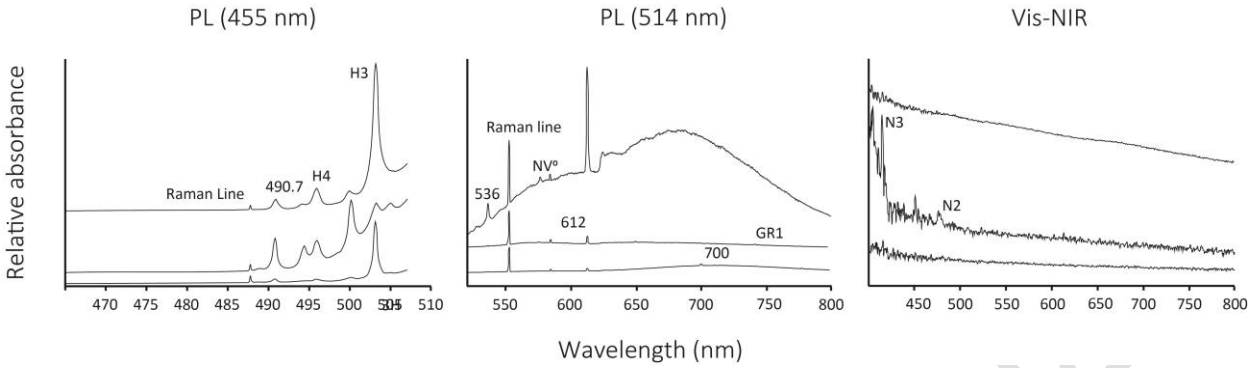

Figure 7A) N_A versus N_B concentration obtained by calculation from infrared absorption spectra. Most diamonds examined for this study preserve more B aggregation and thus plot above the

A=B aggregation line. 7B) Integrated area of absorbance at 3107 cm^{-1} versus N_B concentration. Note most diamonds from the USA always plots below the expected upper limit for a given N_B concentration of diamonds from a global database (thin line) (e.g. Melton 2013; Stachel et al., 2018). Diamond aggregation state could indicate exposure to elevated mantle temperatures.

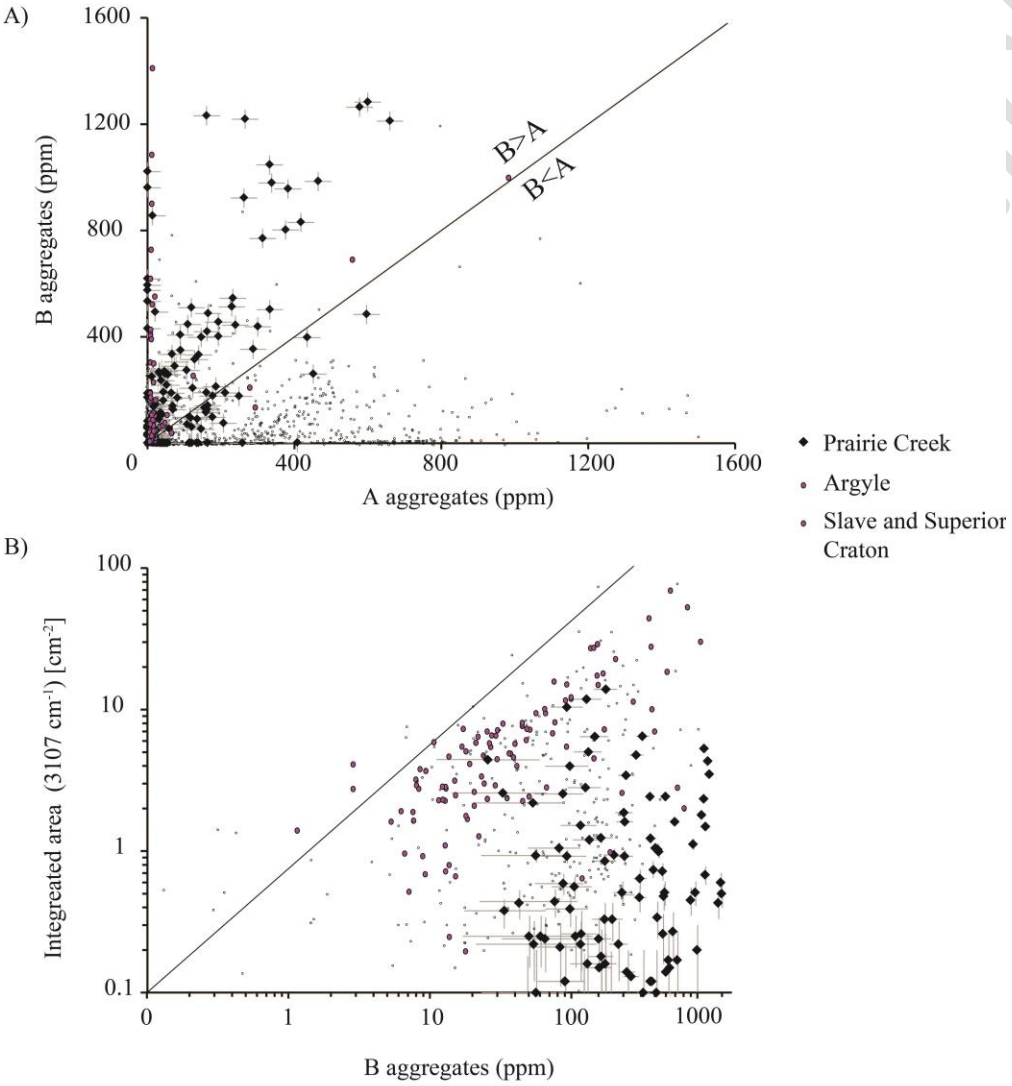

Figure 8. Total nitrogen (at.ppm) versus $\%N_B$ with model isotherms calculated from the aggregation of diamond A aggregates to B aggregates and an assumed age of formation of 1.4

Ga (assuming a mean formation age of 1.4 Ga between 1.6 Ga and 1.2 Ga or analogous to the inferred age of the SCLM of the Yavapai-Mazatzal terrane (Alibert and Albarède 1989, Lambert et al., 1995; Duke et al., 2014) and an eruption age of 110 Ma. White diamond symbols represent IaB diamonds (100% B aggregation) and assume 99% B aggregation, which plot along a minimum ~1290 °C isotherm (Naeser and McCallum 1977; Zartman 1977, Gogineni et al., 1978; Westerlund et al., 2006).

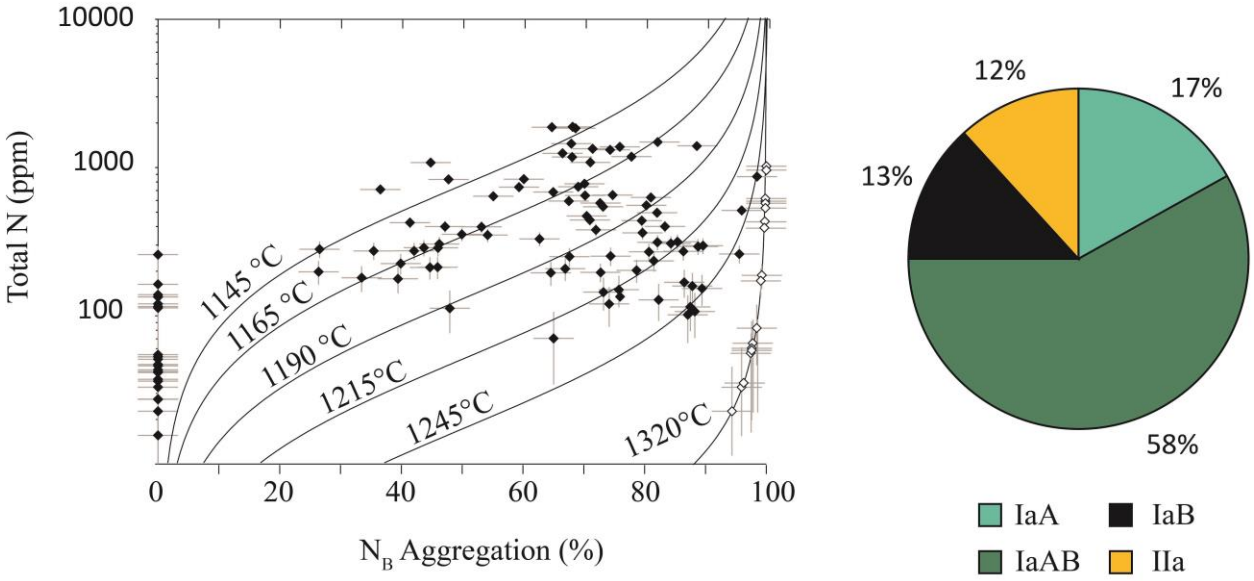

Figure 9. Elastic thermobarometry of forsterite and coesite entrapment conditions in Arkansas diamonds and previous thermobarometric estimates of diamond inclusions and Cr-diopside

mantle xenocrysts from Argyle, Australia (Jaques et al., 1989; Jaques et al., 1994; Stachel et al., 2018; Jaques et al., 2018; Sudholz et al., 2023) and garnet lherzolite and websterite xenoliths from Prairie Creek, USA (Dunn 2002). Also included are estimated paleo-geotherms of the Slave (Kopylova et al., 1999) and Siberian Craton (Dymshits et al., 2020), using the parameters of Hasterok and Chapman (2011). 1σ standard error of ~0.6 GPa. Graphite to diamond transition line modified from Day (2012). Adiabat based on mantle potential temperatures of 1300-1400°C

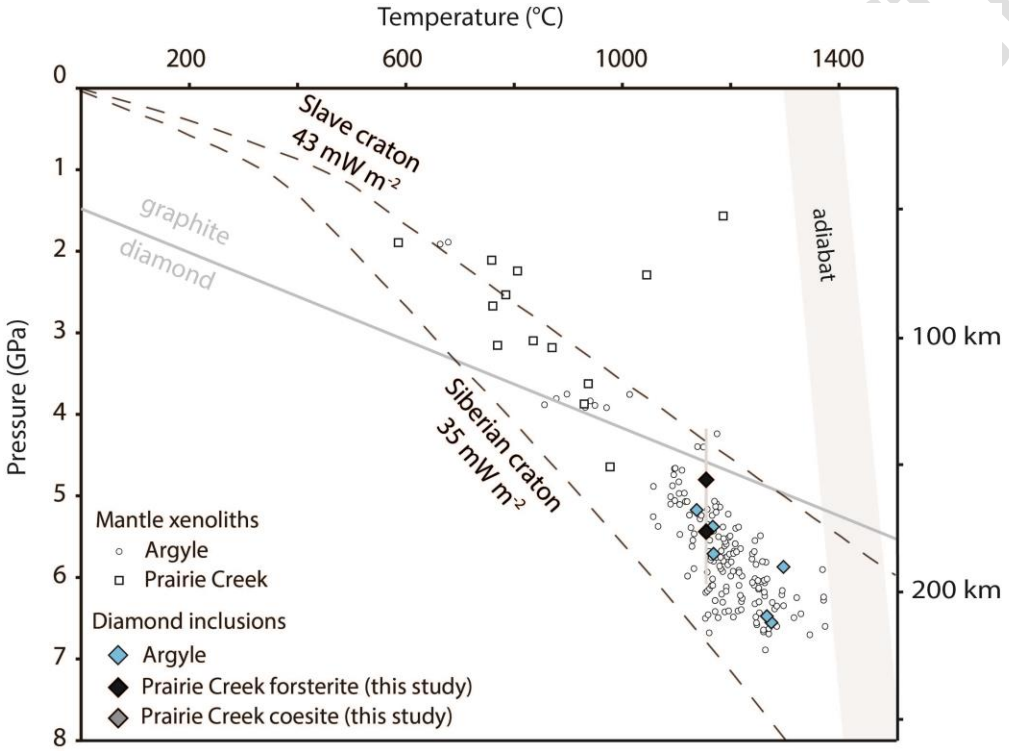

Figure 10. $\delta^{13}C$ compositions of diamonds from the Arkansas compared to those from Argyle (Stachel et al., 2022 and references therein). Peridotite and eclogite ranges adapted from

Cartigny (2005).

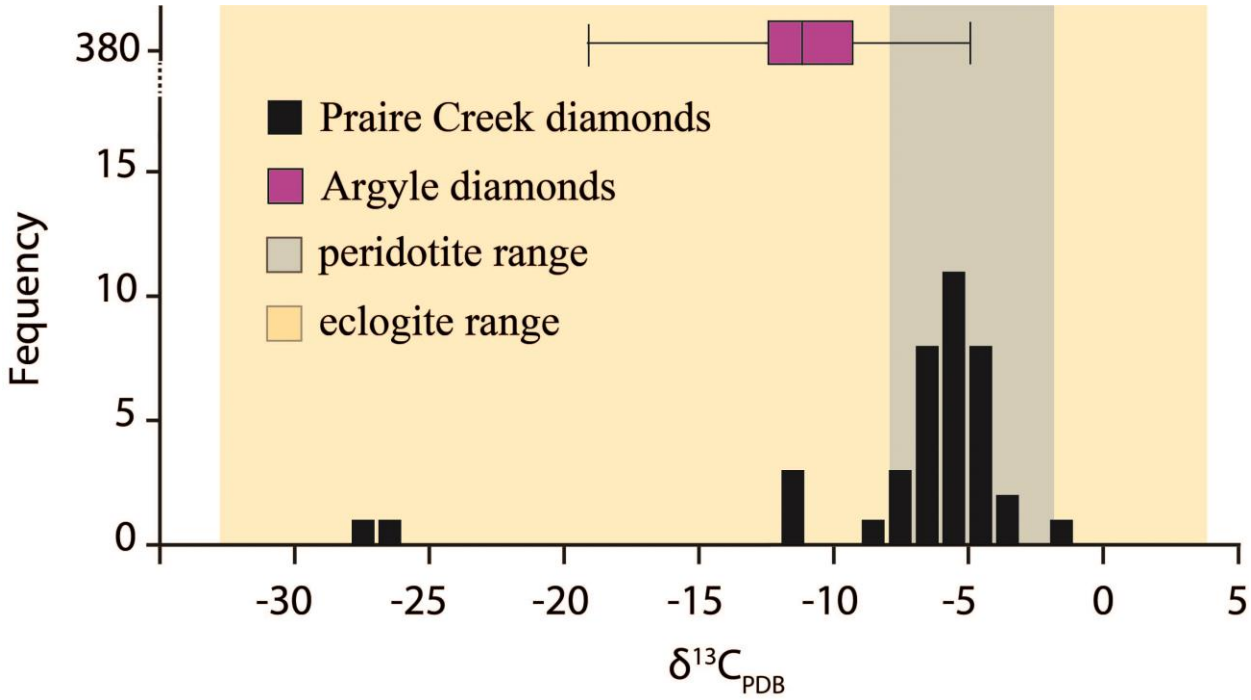

List of Tables

Table 2. Percentage of diamonds with emission peaks detected by photoluminescence spectroscopy.

Table 3. Percentage of diamonds with select visible – near infrared spectral emission features.

Table 4. Summary of calculated residual pressures of forsterite and coesite inclusions in diamonds.

Table 5. Summary geochemistry of Arkansas diamond inclusions from the literature.

Table A1. Summary of incompatible elements of Arkansas diamond inclusions compared to global sources.

Table 1. Summary of physical, infrared, and luminescence characteristics of Arkansas diamonds

Sample	Location	Habit	Color	Type	N_A (ppm)	N_B (ppm)	N_C (ppm)	N total (ppm)[1]	% N_B[2]	% N_C[2]	3107 cm^{-1} peak area (cm^{-2})	Residence T (°C)[3]	CL response color	Inclusions

1	Arkansas	dodecahedron	colorless	IaAB	263	922	-	1185	78	-	1.80	1158	green-blue	
2	Arkansas	flattened dodecahedron	colorless	IaB$_4$	-	35	-	35	100	-	2.57	1320	green-blue	
3	Arkansas	dodecahedron	colorless	IaA	27	-	-	27	-	-	0.83	unknown	green	clinopyroxene, magnetite
4	Arkansas	unknown	colorless	IaB$_4$	-	65	-	65	100	-	0.25	1321	green-blue	
5	Arkansas	combination	colorless	IaAB	596	484	-	1081	45	-	0.72	1125	green-blue	
6	Arkansas	flattened dodecahedron	colorless	IaA	116	-	-	116	-	-	1.77	unknown	green	
7	Arkansas	combination	colorless	IaA	19	-	-	19	-	-	0.19	-	green-blue	
8	Arkansas	combination	colorless	IaAB	120	60	-	181	33	-	0.10	1157	green-blue	
9	Arkansas	flattened dodecahedron	brown	IaAB	13	856	-	869	98	-	0.20	1244	blue	magnetite
10	Arkansas	dodecahedron	yellow	IaAB	193	455	-	648	70	-	0.99	1164	blue	
11	*Arkansas*	*combination*	*colorless*	IaAB	*32*	*101*	-	*133*	*76*	-	10.14	*1213*	*no response*	
12	Arkansas	combination	colorless	IaAB	58	54	-	112	48	-	0.25	1184	blue	
13	*Arkansas*	*dodecahedron*	*brown*	*IIa*	-	-	-	-	-	-	0.51	-	*green-blue*	
14	Arkansas	unknown	colorless	IaA	10	-	-	10	-	-	<0.05	-	green-blue	
15	Arkansas	dodecahedron	yellow	IaAB	333	502	-	835	60	-	0.51	1146	green-blue	
17	Arkansas	flattened dodecahedron	brown	IaB$_4$	-	187	-	187	100	-	0.33	1321	green-blue	
18	Arkansas	flattened dodecahedron	colorless	IaB$_4$	-	1021	-	1021	100	-	4.33	1321	green-blue	
19	Arkansas	flattened dodecahedron	brown	IaAB	164	141	-	305	46	-	0.16	1157	green-blue	
20	Arkansas	dodecahedron	brown	IaAB	314	770	-	1084	71	-	0.45	1152	green-blue	coesite
22	Arkansas	flattened dodecahedron	brown	IaAB	36	114	-	150	76	-	0.56	1209	green	
23	Arkansas	dodecahedron	brown	IaB$_4$	-	618	-	618	100	-	0.17	1321	green-blue	
24	Arkansas	dodecahedron	colorless	IaB$_4$	-	575	-	575	100	-	0.27	1321	green-blue	
25	Arkansas	dodecahedron	colorless	IaAB	14	101	-	115	88	-	0.92	1239	green-blue	
27	*Arkansas*	*dodecahedron*	*colorless*	*IaAB*	*53*	*142*	-	*196*	*73*	-	4.96	*1198*	*green-blue*	
28	Arkansas	dodecahedron	brown	IaAB	376	802	-	1178	68	-	1.12	1146	green-blue	clinopyroxene
29	Arkansas	dodecahedron	colorless	IaAB	21	493	-	514	96	-	0.48	1231	green-blue	
30	Arkansas	unknown	colorless	IaA	15	-	-	15	-	-	<0.05	-	green-blue	
31	Arkansas	unknown	colorless	IaAB	155	132	-	287	46	-	0.06	1158	green-blue	
32	Arkansas	combination	colorless	IaB$_4$	-	961	-	961	100	-	5.30	1321	green-blue	
33	Arkansas	combination	colorless	IaA	56	-	-	56	-	-	0.05	-	green-blue	
34	Arkansas	flattened dodecahedron	yellow	IaAB	660	1212	-	1871	65	-	0.43	1131	no response	
35	Arkansas	combination	colorless	IaA	134	-	-	134	-	-	0.18	-	green-blue	
36	Arkansas	flattened dodecahedron	brown	IaAB	211	189	-	400	47	-	0.16	1151	green-blue	
37	Arkansas	combination	colorless	IaAB	239	444	-	683	65	-	0.34	1156	green-blue	
38	*Arkansas*	*unknown*	*colorless*	*IaB$_4$*	-	*391*	-	*391*	*100*	-	2.40	*1321*	*green-blue*	
39	Arkansas	flattened dodecahedron	yellow	IaAB	600	1283	-	1882	68	-	0.50	1135	green-blue	
40	Arkansas	unknown	colorless	IaAB	249	176	-	425	41	-	1.24	1144	blue	
41	Arkansas	unknown	colorless	IaB$_4$	-	533	-	533	100	-	0.17	1321	green-blue	
42	Arkansas	dodecahedron	colorless	IaAB	117	95	-	212	45	-	0.59	1165	green-blue	
44	Arkansas	unknown	colorless	IaA	134	-	-	134	-	-	<0.05	-	green-blue	

45	Arkansas	unknown	brown	IaB$_4$	-	58	-	58	100	-	2.19	1291	green-blue	
46	Arkansas	flattened dodecahedron	yellow	IaAB	382	957	-	1339	71	-	2.34	1125	no response	
47	Arkansas	flattened dodecahedron	brown	IaA	37	-	-	37	-	-	0.70	-	blue	
48	*Arkansas*	*unknown*	*colorless*	*IaAB*	*157*	*1235*	-	*1392*	*89*	-	2.74	*1175*	*no response*	
49	Arkansas	unknown	brown	IIa	-	-	-	-	-	-	0.31	-	green	
50	Arkansas	flattened dodecahedron	colorless	IIa	-	-	-	-	-	-	<0.05	-	blue	
51	Arkansas	unknown	colorless	IaB$_4$	-	594	-	594	100	-	1.61	1321	green-blue	
52	Arkansas	flattened dodecahedron	colorless	IIa	-	-	-	-	-	-	0.51	-	green	
53	Arkansas	flattened dodecahedron	brown	IaA	-	33	-	33	-	-	<0.05	-	green	
54	Arkansas	dodecahedron	brown	IaAB	56	257	-	313	82	-	1.87	1200	no response	
55	*Arkansas*	*flattened dodecahedron*	*yellow*	*IaAB*	*263*	*1223*	-	*1486*	*82*	-	1.42	*1160*	*green-blue*	
56	Arkansas	dodecahedron	yellow	IaAB	110	447	-	556	80	-	1.03	1182	green	
57	Arkansas	dodecahedron	brown	IaAB	23	146	-	168	87	-	1.20	1226	green	
58	Arkansas	dodecahedron	yellow	IaAB	332	1047	-	1379	76	-	3.50	1152	green-blue	
59	Arkansas	unknown	colorless	IaA	51	-	-	51	-	-	0.49	-	green	
60	Arkansas	flattened dodecahedron	colorless	IaA	47	-	-	47	-	-	<0.05	-	green	
61	Arkansas	unknown	colorless	IaA	33	-	-	33	-	-	0.32	-	green	
62	*Arkansas*	*flattened dodecahedron*	*colorless*	*IaA*	*175*	-	-	*175*	-	-	0.09	-	*green-blue*	
63	Arkansas	flattened dodecahedron	colorless	IaAB	123	207	-	330	63	-	0.08	1172	blue	
64	Arkansas	combination	colorless	IaAB	578	1264	-	1842	69	-	0.60	1136	green-blue	
65	Arkansas	unknown	colorless	IaAB	435	397	-	832	48	-	0.12	1134	blue	
66	Arkansas	flattened dodecahedron	colorless	IaA	42	-	-	42	-	-	0.15	-	green-blue	
67	Arkansas	combination	colorless	IaAB	25	46	-	70	65	-	0.43	1216	green	
68	Arkansas	flattened dodecahedron	colorless	IaB$_4$	-	171	-	171	100	-	0.15	1321	green	
69	*Arkansas*	*combination*	*yellow*	*IaAB*	*157*	*418*	-	*576*	*73*	-	0.74	*1170*	*green-blue*	
70	Arkansas	flattened dodecahedron	colorless	IaAB	465	985	-	1449	68	-	1.49	1141	no response	
ARM1	Arkansas	dodecahedron	brown	IIa	-	-	-	-	-	-	0.30	-	green	
ARM10	Arkansas	dodecahedron	colorless	IaAB	43	160	-	203	79	-	6.44	1206	green-blue	
ARM11	Arkansas	dodecahedron	brown	IaAB	39	106	-	144	73	-	0.39	1207	green	
ARM12	Arkansas	dodecahedron	brown	IaAB	288	353	-	641	55	-	0.10	1148	blue	
ARM13	Arkansas	dodecahedron	brown	IaA	16	-	-	16	-	-	0.37	-	green	
ARM15	Arkansas	dodecahedron	brown	Ib/IaA	143	-	107	250	-	57	0.15	-	green-blue	
ARM16	Arkansas	flattened dodecahedron	brown	IaA	163	-	-	163	-	-	<0.05	-	green	
ARM2	Arkansas	dodecahedron	brown	IaAB	90	349	-	439	80	-	6.48	1186	green-blue	
ARM3	Arkansas	dodecahedron	brown	IaAB	69	139	-	208	67	-	11.85	1189	green-blue	
ARM4	Arkansas	dodecahedron	colorless	IaA	120	-	-	120	-	-	0.67	-	green	olivine
ARM5	Arkansas	dodecahedron	colorless	IaB$_4$	-	36	-	36	100	-	0.38	1320	green	olivine
ARM6	Arkansas	dodecahedron	brown	IaAB	146	398	-	544	73	-	1.23	1172	green-blue	
ARM7	Arkansas	dodecahedron	brown	IaAB	177	177	-	354	50	-	0.18	1157	green	
ARM8	Arkansas	flattened dodecahedron	brown	-	-	-	-	-	-	-	-	-	green-blue	

ARM9	Arkansas	dodecahedron	brown	IaAB	177	97	-	274	35	-	0.12	1149	green-blue	
BL01	Arkansas	dodecahedron	colorless	IaA	259	-	-	259	-	-	<0.05	-	-	
BL02	Arkansas	octahedron	colorless	Ib	-	-	28	28	-	100	<0.05	-	blue	
BL1_4	Arkansas	octahedron	colorless	IIa	-	-	-	-	-	-	0.11	-	-	clinopyroxene, rutile
COD001	Arkansas	dodecahedron	brown	IaAB	12	249	-	261	96	-	0.51	1247	green	
COD002	Arkansas	flattened dodecahedron	colorless	IaAB	52	218	-	270	81	-	0.94	1201	blue	
COD003	Arkansas	dodecahedron	colorless	IaAB	65	188	-	253	74	-	0.85	1193	blue	graphite
COD004	Arkansas	octahedron	brown	IaAB	23	106	-	128	82	-	3.98	1224	blue	
GW_7_11_09	Arkansas	octahedron	brown	IaAB	159	116	-	274	42	-	0.25	1156	-	
GW_8_8_14	Arkansas	dodecahedron	yellow	IaAB	418	831	-	1248	67	-	0.51	1143	-	
TK01	Arkansas	octahedron	colorless	IIa	-	-	-	-	-	-	0.13	-	-	ilmenite
TK02	Arkansas	irregular	colorless	IIa	-	-	-	-	-	-	<0.05	-	-	
AKSK002	Arkansas	dodecahedron	colorless	IaB_4	-	27	-	27	-	-	4.42	1320	-	
AKSK003	Arkansas	dodecahedron	colorless	IaAB	162	126	-	288	44	-	0.22	1156	-	
AKSK004	Arkansas	unknown	colorless	IaAB	33	261	-	294	89	-	1.61	1216	-	
AKSK005	Arkansas	dodecahedron	colorless	IaB_4	0	431	-	431	100	-	1.05	1321	-	
AKSK006	Arkansas	combination	brown	IaAB	74	289	-	363	80	-	0.13	1192	-	
AKSK007	Arkansas	dodecahedron	colorless	IaAB	46	270	-	316	85	-	0.14	1206	-	
AKSK008	Arkansas	dodecahedron	colorless	IaAB	43	191	-	235	82	-	13.90	1206	-	
AKSK009	Arkansas	combination	colorless	IaAB	193	401	-	594	68	-	0.05	1163	-	
AKSK010	Arkansas	flatted dodecahedron	colorless	IaA	139	0	-	139	0	-	0.09	-	-	
AKSK011	Arkansas	flatted dodecahedron	colorless	IaA	36	0	-	36	0	-	-	-	-	
AKSK012	Arkansas	dodecahedron	colorless	IaAB	108	70	-	178	39	-	0.24	1164	-	
AKSK013	Arkansas	irregular	colorless	IIa	0	0	-	0	0	-	0.05	-	-	
AKSK014	Arkansas	combination	colorless	IaA	22	0	-	22	0	-	0.16	-	-	
AKSK015	Arkansas	unknown	colorless	IaB_4	0	56	-	56	100	-	<0.05	1321	-	
AKSK016	Arkansas	unknown	colorless	IaAB	67	334	-	401	83	-	0.64	1195	-	
AKSK017	Arkansas	unknown	colorless	IaAB	106	274	-	380	72	-	0.09	1179	-	
AKSK018	Arkansas	dodecahedron	colorless	IaA	55	0	-	55	0	-	0.83	-	-	
AKSK019	Arkansas	dodecahedron	brown	IaA	39	0	-	39	0	-	0.83	-	-	
AKSK020	Arkansas	dodecahedron	brown	IaAB	31	266	-	297	90	-	3.43	1218	-	
AKSK021	Arkansas	flatted dodecahedron	brown	IaAB	48	259	-	308	84	-	0.92	1204	-	
AKSK022	Arkansas	dodecahedron	brown	IaAB	13	94	-	107	88	-	2.54	1243	-	
AKSK023	Arkansas	flatted dodecahedron	colorless	Ib/IaA	407	-	509	915	-	44	0.53	-	-	
AKSK024	Arkansas	unknown	colorless	IaAB	230	513	-	742	69	-	0.14	1159	-	
AKSK025	Arkansas	dodecahedron	colorless	IaAB	232	545	-	777	70	-	0.15	1159	-	
AKSK026	Arkansas	unknown	brown	IaAB	161	190	-	351	54	-	0.08	1162	-	
AKSK027	Arkansas	unknown	colorless	IaAB	338	979	-	1317	74	-	0.68	1151	-	
AKSK028	Arkansas	dodecahedron	brown	IaA	43	-	-	43	-	-	0.19	-	-	
AKSK029	Arkansas	unknown	brown	IaAB	146	52	-	198	26	-	0.08	1146	-	

AKSK030	Arkansas	flatted dodecahedron	brown	IaA	45	-	-	45	-	-	0.05	-	-
AKSK031	Arkansas	dodecahedron	colorless	IaAB	119	510	-	629	81	-	2.43	1180	-
AKSK032	Arkansas	flatted dodecahedron	brown	IaA	46	-	-	46	-	-	<0.05	-	-
AKSK033	Arkansas	dodecahedron	colorless	IaB[4]	-	82	-	82	100	-	0.44	1321	-
AKSK034	Arkansas	irregular	colorless	IIa	-	-	-	-	-	-	<0.05	-	-
AKSK035	Arkansas	flatted dodecahedron	colorless	IaAB	31	89	-	120	74	-	<0.05	1213	-
AKSK036	Arkansas	flatted dodecahedron	colorless	IaAB	81	170	-	251	68	-	0.24	1185	-
AKSK037	Arkansas	unknown	colorless	IaAB	300	438	-	738	59	-	0.10	1148	-
akgw001-IR	Arkansas	dodecahedron	colorless	IaA	53	-	-	53	-	-	0.21	-	-
aksd-0_39-4608	Arkansas	flatted dodecahedron	yellow	IaAB	139	332	-	471	70	-	0.47	1172	-
aksd-1_28-8605	Arkansas	dodecahedron	brown	IaAB	165	488	-	653	75	-	0.26	1169	-
aksd-2_67_2507	Arkansas	dodecahedron	yellow	IIa	-	-	-	-	-	-	0.29	-	-
aksd-0_51_31308	Arkansas	flatted dodecahedron	yellow	IaAB	16	137	-	153	89	-	2.81	1236	-
aksd-0_99-81390	Arkansas	unknown	yellow	IaB[4]	-	60	-	60	100	-	0.93	1321	-
aksd-2_43-91903	Arkansas	dodecahedron	yellow	IaB[4]	-	58	-	58	100	-	0.22	1321	-
aksd-0_90-6497	Arkansas	unknown	brown	IaAB	89	407	-	496	82	-	0.12	1188	-
aksd-1_43-10203	Arkansas	dodecahedron	yellow	IaAB	37	235	-	272	86	-	0.22	1212	-
aksd-1_24-5505	Arkansas	unknown	colorless	IaA	23	-	-	23	-	-	0.32	-	-
aksd-1_96-3610	Arkansas	irregular	colorless	IIa	-	-	-	-	-	-	<0.05	-	-
aksd-1_56-102011	Arkansas	flatted dodecahedron	colorless	IIa	-	-	-	-	-	-	1.03	-	-
aksd-0_72-22896	Arkansas	irregular	colorless	IIa	-	-	-	-	-	-	<0.05	-	-
aksd-1_79-21822	Arkansas	flatted dodecahedron	colorless	IIa	-	-	-	-	-	-	<0.05	-	-
aksd-8_66-42711	Arkansas	irregular	colorless	IIa	-	-	-	-	-	-	<0.05	-	-
DR-0_91	Arkansas	irregular	colorless	IIa	-	-	-	-	-	-	0.53	-	-
DR-0_28	Arkansas	irregular	colorless	IIa	-	-	-	-	-	-	<0.05	-	-
DR-0_27	Arkansas	irregular	colorless	IIa	-	-	-	-	-	-	<0.05	-	-
DR-0_12br	Arkansas	unknown	brown	IaAB	207	75	-	281	27	-	<0.05	1138	-
DR-0_11	Arkansas	unknown	colorless	IaA	113	-	-	113	-	-	0.21	-	-
DR-0_10br	Arkansas	unknown	brown	IaAB	186	212	-	398	53	-	0.33	1157	-
DR-0_07y	Arkansas	unknown	yellow	IaAB	13	89	-	102	87	-	1.05	1241	-
DR-0_07a-11-17-18	Arkansas	unknown	colorless	IaAB	115	98	-	213	46	-	0.12	1166	-
AKCZ001	Arkansas	dodecahedron	brown	IaAB	19	140	-	159	88	-	-	1230	-
AKDR001	Arkansas	dodecahedron	brown	IaA	42	-	-	42	-	-	-	-	-
AKTP002	Arkansas	dodecahedron	brown	IaAB	69	126	-	195	65	-	0.26	1188	-
AKSK068	Arkansas	dodecahedron	colorless	IaAB	128	314	-	443	71	-	4.77	1174	-

[1]2σ - 64 ppm, [2]2σ - 4%, [3]assuming an eruption age of; 102 Ma (Zartman, 1977, Gogineni et al., 1978) and residence time of 3.2 Ga for the Praire Creek lamproite. Nitrogen concentration was calculated from individual spectra by applying the Beer-Lambert law and absorption values of nitrogen bands at 1365, 1284, and 1175 cm^{-1}, using the least-squares fitting approach combined with a basic linear correction in the DiaMap excel spreadsheet (e.g., Howell et al., 2012a, 2012b). [3]2σ = 62 °C, and a mean assumed formation age of 1.4 between 1.6 and 1.4 Ga or the inferred age of Yavapai-Mazatzal terrane (Alibert and Albarede 1989, Lambert et al., 1995; Duke et al., 2014), and therefore residence time of 1.3 Ga.. Italized rows reflect oversaturated and therefore minimum estimates. [4]IaB minimum diamond residence temperatures assuming a 99% B aggregation state. Inclusions were identified by comparing Raman spectra with known representatives in the Ruff Database (LaFuente et al.,2016) and supplemented with morphology, color, texture, and other optical properties

Table 2. Percentage of Arkansas diamonds with select vis-NIR emission features

Peak position (nm)	% of diamonds	Defect	Defect Species	Impurity/Cause
415.2	14%	N_3V	Cape	Nitrogen[1]
503.2	0%	$(NVN)^0$	H3	Nitrogen[2]
550	6%	-	550 nm band	Plastic deformation[1,3]
741	0%	V^0	GR1	Radiation[4]
835	0%	-	H-band	Hydrogen[1,5]
-	72%	-	Featureless	-

N - Nitrogen, C - Carbon, V^0 - neutral vacancy, [1]Zaitsev, 2010 and references therein, [2]Sobolev and Lisoivan, 1971, [3]Bokii et al., 1986, [4]Shigley and Breeding, 2013, [5]Breeding et al., 2018

Table 3. Summary of residual pressures of forsterite, coesite, and diopside inclusions in Arkansas diamonds

Sample	Location	Mineral	Length (µm)	Width (µm)	Entrapped peaks (cm^{-1})[1]	Residual P (GPa)[2]	Mean Mantle residence T (ºC)[3]	Entrapment P (GPa)
ARM4_incl01	Arkansas	forsterite	8	5	855.17	0.26	1205	5.00
ARM5_incl01	Arkansas	forsterite	20	20	856.33	0.64	1320	5.42
20_incl01	Arkansas	coesite	50	50	528.58	2.61	1152	-
					467.70	2.58		-
					426.90	-0.22		-
					354.25	-0.17		-

[1]relative to 854.36 cm^{-1} of San Carlos olivine Fo_{90} (Abramson et al., 1997) for forsterite, relative to 521 cm^{-1} of synthetic coesite (Sobolev et al., 2000), [2]Assuming a 3.09 cm^{-1} per GPa (Wang et al., 1993) for forserite and 2.9 cm^{-1}, 0.66 cm^{-1}, 0.45 cm^{-1}, 0.44 cm^{-1} per GPa for the Raman bands 521 cm^{-1}, 466 cm^{-1}, 427 cm^{-1}, 355 cm^{-1} respectively (Hemley et al., 1984; Sobolev et al., 2000) for coesite, [3]2σ = 62 °C, assuming an eruption age of 102 Ma (Zartman, 1977, Gogineni et al., 1978), and a mean assumed formation age of 1.4 between 1.6 and 1.4 Ga or the inferred age of Yavapai-Mazatzal terrane (Alibert and Albarede 1989, Lambert et al., 1995; Duke et al., 2014), and therefore residence time of 1.3 Ga. Nitrogen concentration was calculated from individual spectra by applying the Beer-Lambert law and absorption values of nitrogen bands at 1365, 1284, and 1175 cm^{-1}, using the least-squares fitting approach combined with a basic linear correction in the DiaMap excel spreadsheet (e.g., Howell et al., 2012a, 2012b).

Table A1. Incompatible elements in an Arkansas clinopyroxene compared to global sources

Oxide (wt.%)	E type clinopyroxene[1]	P type clinopyroxene[1]	Arkansas clinopyroxene[3]
Na_2O	4.62±1.89	1.32±1.20	2.85
K_2O	0.29±0.29	0.18±0.23	0.15
TiO_2	0.45±0.21	0.14±0.26	0.31
Na/(Na+Ca)[3]	0.38±0.14	0.11±0.09	0.27

[1]Stachel et al 2022 and references therein, [2]Newton et al., 1977, [3]Clarke and Papike 1968